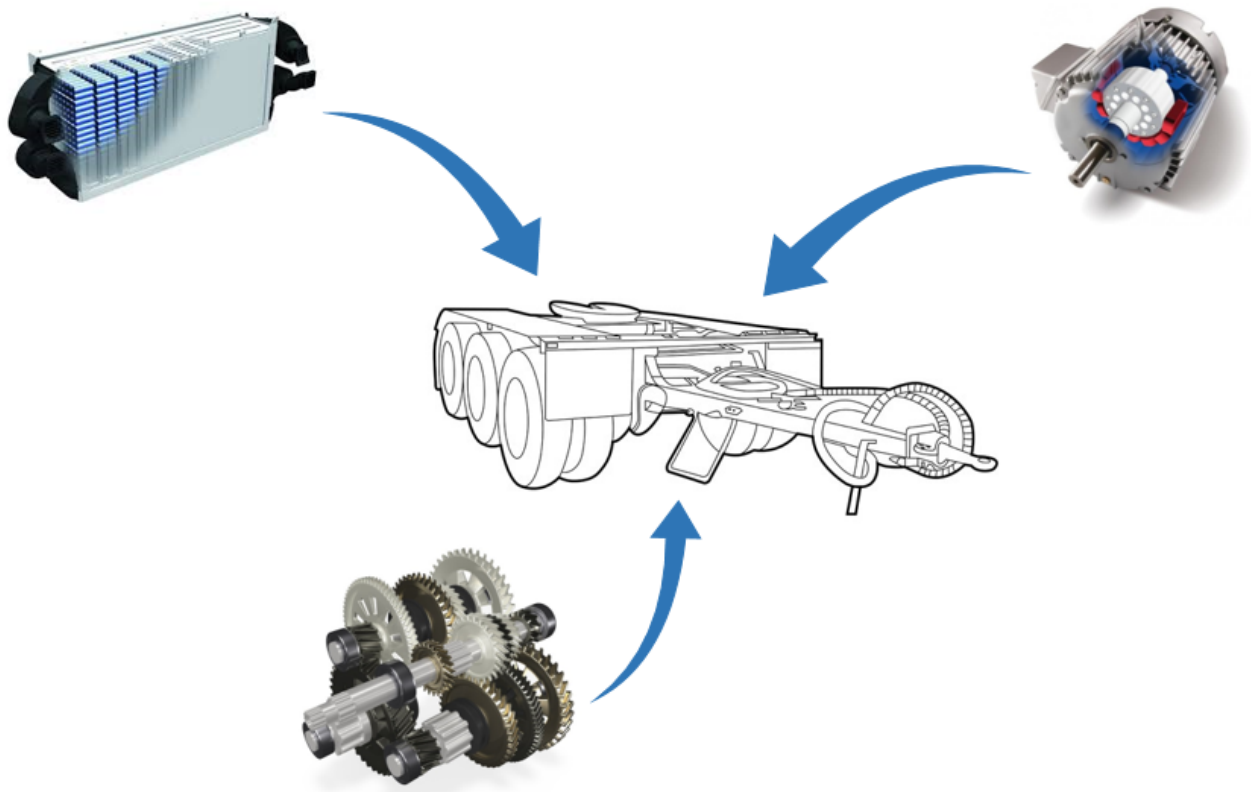
CHALMERS



Energy consumption, Performance and Stability Analysis of Articulated Vehicles Powered with Electrified Dolly

Master's thesis

IURI PEREIRA BARROS

Department of Mechanics and Maritime Sciences
CHALMERS UNIVERSITY OF TECHNOLOGY
Göteborg, Sweden 2018

MASTER'S THESIS

Energy consumption, Performance and Stability Analysis of Articulated Vehicles Powered with Electrified Dolly

IURI PEREIRA BARROS

Department of Mechanics and Maritime Sciences
Division of Vehicle Engineering and Autonomous Systems
CHALMERS UNIVERSITY OF TECHNOLOGY

Göteborg, Sweden 2018

Energy consumption, Performance and Stability Analysis of Articulated Vehicles Powered with Electrified Dolly
IURI PEREIRA BARROS

© IURI PEREIRA BARROS, 2018

Master's thesis 2018:61
Department of Mechanics and Maritime Sciences
Division of Vehicle Engineering and Autonomous Systems
Chalmers University of Technology
SE-412 96 Göteborg
Sweden
Telephone: +46 (0)31-772 1000

Cover:
Representation of a dolly that posses an electric propulsion system (EPS), i.e. battery, transmission and electric motor named e-dolly.

Chalmers Reproservice
Göteborg, Sweden 2018

Energy consumption, Performance and Stability Analysis of Articulated Vehicles Powered with Electrified Dolly
Master's thesis
IURI PEREIRA BARROS
Department of Mechanics and Maritime Sciences
Division of Vehicle Engineering and Autonomous Systems
Chalmers University of Technology

Abstract

Regarding the emission of greenhouse gases by economic activity, transportation is accounted for almost 25.8% of these emitted pollutants [1]. Moreover, the majority part of these emissions are derived from vehicles powered with Internal Combustion Engines (ICEs). To avoid future complications due to air contamination, e.g. global warming and health issues, most countries are proposing harder restrictions on vehicle emission standards. Therefore, the search for sustainable drive-trains is in the spotlight of today's automotive industry agenda. Hybridization of conventional fossil fuel trucks, using electrified dolly, appears as a candidate solution for the problem. Unlike conventional dollies, the electrified dolly posses an electric propulsion system (i.e. batteries and electric drive), which makes it capable of propelling its own axle and aid the tractor unit to move the system. As a consequence of this additional power source, the combination truck becomes a hybrid vehicle.

Considering that electrified dolly is a new trend in the industry and few studies were performed on this topic, the benefits and drawbacks of the product are not well known. Hereupon, this work aims, via simulation, to assess the potential impact of the e-dolly technology on vehicle's performance, fuel efficiency and dynamic stability. Furthermore, to verify how power split decisions, made by a control unit of a hybrid vehicle, are affected when lateral stability constraints or drawbar constraints are included in the control algorithm.

The objects of study are A-doubles, a class of long haul articulated vehicles, with Gross Combination Weight (GCW) of 60 and 80 tonnes. Models are proposed to simulate vehicle's longitudinal and lateral dynamics along with the control algorithm that is responsible to perform the power split decisions of the hybrid architecture. The Energy Management Strategy (EMS) of the controller is based on an adaptive Equivalent Consumption Minimization Strategy (ECMS) approach.

Keywords: A-double, electrified dolly, energy consumption, fuel consumption, heavy duty, hybrid, optimization, stability, truck

Acknowledgements

During this work I faced many challenges, but for each challenge a friend, in or out of this thesis project, helped me to overcome them. Here, I would like to thank those people. First, for all the knowledge, insights, discussions and feedbacks I thank you examiner and supervisors at Chalmers, Bengt Jacobson, Pär Pettersson and Toheed Ghandriz. Despite my sudden arrival at the VEAS department and the large workload that I brought to us, I appreciate the friendly welcome, guidance and time spent with me answering this thesis work questions.

For those that I met at Volvo Trucks, I would like to thank, from the Swedish site, Tobias Axelsson, Anders Eriksson and Sixten Berglund for the opportunity offered to me. Also, for those who guided me from an industrial perspective, even if a little, I thank Jonas Hellgren, Rickard Andersson and Erik Jonsson. From the Brazilian site, I would like to thank Roberson Assis and to highlight the names of Rodrigo Bru and Allan Charello, these two have made a major influence on my career, allowing and supporting my decision to take the exchange to Chalmers University and perform this thesis work, even if it meant to start a new intern selection process and every painful bureaucracy related to it, thank you very much. My last thanks, in this paragraph, goes to Rafael Smijtink who helped me in both Brazilian and Swedish sites of Volvo Trucks, thank you very much for all the support and discussion in this work.

In this last paragraph I would like to express my sincere gratitude to the people that aided me before and after my arrival, and in every aspect of my staying in Sweden. The help in personal matters and every invitation to join you guys somewhere ensured me happy moments. They are, Rafael Smijtink (yes, again), André and Claudia Klostermann, and Lucas Araujo. You turned out to be truly friends and your kindness cannot be expressed within this short acknowledgement, thank you. My final remarks goes to my friends from the Master' Thesis room in the VEAS department, who endured me for half of this journey and provided me good laughs. And finally to Ing-Britt Carlsson that, along with my home university (UTFPR), made this exchange possible.

Contents

Abstract i

Acknowledgements ii

Contents iii

1 Introduction 1
1.1 Background . . . 1
1.2 Challenge . . . 2
1.3 Scope . . . 2
1.4 Goals and Limitations . . . 3
1.5 Outline . . . 3

2 Transport Mission 4

3 Vehicle Longitudinal Model 5
3.1 Energy Storage System . . . 5
3.1.1 State of Charge . . . 6
3.1.2 State of Health . . . 6
3.2 Energy Management Strategy . . . 7
3.2.1 Objective Function . . . 7
3.2.2 Optimization Framework . . . 9
3.2.3 Constraints . . . 10
3.2.4 Determining the Equivalence Factor . . . 12

4 Vehicle Lateral Model 15
4.1 Vectorized model . . . 15
4.2 Strategy for Vehicle Stability Analysis . . . 16
4.3 Implementation of the FMU . . . 17

5 Model Validation 18

6 Results and Discussion 21
6.1 A Comparison on Fuel Consumption . . . 21
6.2 A Comparison on Vehicle Performance . . . 23
6.3 A Comparison on Vehicle Stability . . . 26
6.4 The Influence of the Stability Constraint on Control Decisions . . . 29
6.5 The Influence of Drawbar Limitations on the Control Decision . . . 31

7 Conclusion 34

8 Future Work 35

References 36

Appendix A Data 38

Appendix B Drawbar Constraint 39

1 Introduction

1.1 Background

Dollies are usual in Long Combination Vehicles (LCVs) to attach full trailers and semi-trailers to the main tractor unit, which allows them to transport additional freight. Studies regarding converter dolly electrification are now being performed with the objective of hybridizing diesel-powered LCVs. A brief elucidation is exposed in the following content in order to understand the scope and challenge related to this subject.

To avoid road damage most countries limit the amount of cargo tied to a truck by its number of axles. In order to comply with the norms and depending on the user's needs, a dolly might be used to overcome these restrictions. A conventional dolly can be shortly described as a platform coupled with unpowered wheels that attaches towed units to a truck with strong traction capacity (Fig. 1.1), doing so, the cargo does not need to be fully placed over the main truck chassis, but rather distributed over the extra axles provided by dolly and trailer units.

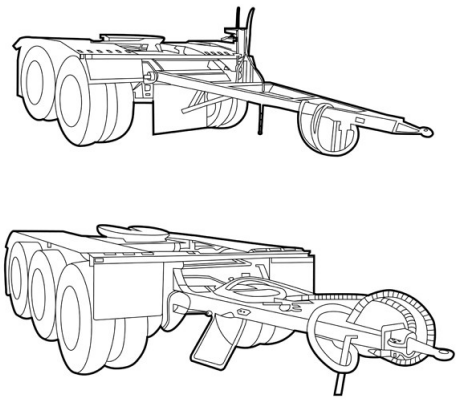


Figure 1.1: *Conventional dolly used in long articulated vehicles [2].*

To transport heavy freights and achieve satisfactory vehicle performance, e.g. range, grade-ability and acceleration, the truck is traditionally powered with a robust ICE. However, the amount of fuel required to operate a combustion engine is directly proportional to its size (in litre) and so is the pollutant formation from the fuel combustion. Hence, to perform a transport task with this high sized engines, large amounts of fuel would be required, which in turns would also produce large amounts of pollutant. Knowing that international policies are gradually restricting the emission limit of greenhouse gases for road vehicles [2], it is necessary to improve their propulsion system in a way that affords lower fuel consumption.

Optimization can be performed in many systems and fields, for example, one could implement lighter materials on gearbox housings or improve heat exchange on the fuel combustion process. Unfortunately, since several researches were made with the intention to enhance standard combustion vehicles and that succeeded in doing so, the difficulty to improve conventional hardware has become higher and the eligible spots/rewards lower.

Hybridization of ICE trucks, through dolly electrification, appears as a candidate solution to this problem. Properly controlled hybrids leads to reduced fuel consumption and ownership cost in the long run. The electrified dolly, or e-dolly for short, has an Electric Propulsion System (EPS) integrated to its hardware. The main advantage of this feature is the possibility of truck hybridization without affecting the prime mover design, but rather its software. Also, Plug-in HEVs allow battery recharge from the electric grid and offer a significant range in pure electric mode, which might be necessary due to legislation. Stated the key element that fostered this work, the thesis' challenge and scope can now be described.

1.2 Challenge

Hybrid electric vehicles posses two or more power sources to provide traction for the wheels, usually one combustion engine and one electric machine. The existence of multiple sources within the same architecture raises a challenging task defined as the Optimal Control Problem (OCP). It can be described, in its most general form, as finding the set of actions ($\mathbf{u}(t)$) that minimizes the fuel consumption (m_f) of a vehicle within a time interval ($t_i \leq t \leq t_f$), as demonstrated in Eq. 1.1. The action u determines how the power demanded from the driver (P_{dem}) will be split between the available propulsion systems. Function J, also known as cost function, can be designed to account many properties of interest, e.g. CO_2 emissions [3] and total energy consumption [4].

$$J = \int_{t_i}^{t_f} \dot{m}_f(u(t), t)dt \tag{1.1}$$

To solve this problem, an Energy Management Strategy (EMS) is used by the control unit to give a solution for the OCP, but there are many approaches to perform it. Furthermore, a truck propelled in two different spots can be subjected to jack-knifing or spin-out if, for instance, the rear-end drive provides too much traction to the wheels while cornering. Also, a wrong brake distribution can lead to steering instability of the front wheels [5]. Therefore, the controller must be able to evaluate the consequences of each power split decision made by the EMS with a representative model of the vehicle dynamics. However, it must be simple enough to be implemented within the controller without increasing the control units' run time excessively. For these purposes, the challenge is to select the proper technique to compute the split decision given a vehicle set-up and a transport task.

1.3 Scope

This research's objective is to determine the pros and cons of e-dolly hybrid vehicles in comparison to conventional diesel trucks while performing the same Operating Cycle (OC). More specifically, evaluate the performance on energy efficiency (i.e fuel consumption), average speed, road gradeability and lateral stability of an A-double truck with different hardware set-up and weight. Also, two control policies, one that takes into account lateral stability and the other that does not, will be compared. The hardware may vary in engine size and battery type, here 11, 13 and 16 litres diesel engines plus 2 power- and 3 energy-optimized batteries are used. Regarding vehicle weight, loaded gross mass of 60 and 80 tonnes are assessed. For the 80 tons case, a D16 powered vehicle will be compared with a D13 plus e-dolly. With respect to the 60 tons, a D13 truck will be compared to a D11 plus e-dolly combination. This investigation will verify how trucks with downsized internal combustion engine coupled with an electrified dolly behaves in comparison to a standard diesel-powered trucks.

An A-double is a four units articulated vehicle that consists, respectively, of tractor, semi-trailer, converter dolly and other semi-trailer. These two trailers are connected by the dolly (Fig. 1.2). The LCV in consideration has five (5) groups of axle and eleven (11) axles.

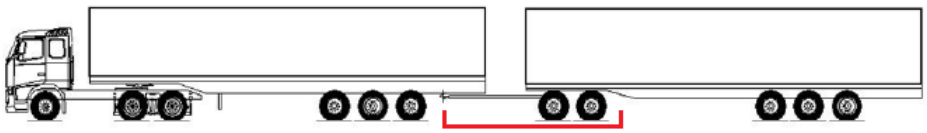


Figure 1.2: *A-double combination truck with converter dolly [6]. The bracket shows where the converter dolly is placed in the combination vehicle.*

Besides lateral stability, the remaining criteria for rating truck's performance is evaluated in a modular forward simulation, shown in Fig. 1.3, of the vehicle longitudinal dynamics. Simulink environment is used to mimic vehicle components and Matlab to solve the instantaneous optimization problem. Lateral dynamics will be simulated in Dymola environment using Modelica language. Further details and reasoning will be displayed latter in this thesis. The models will be joined together with a Functional Mock-up Interface (FMU).

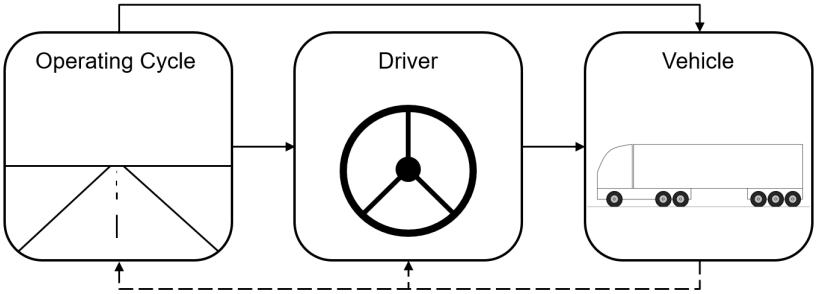


Figure 1.3: *The main frame of a forward simulation with 3 main models, the operating cycle, the driver and the vehicle. Arrows represent signal flow. This picture was inspired in [7].*

1.4 Goals and Limitations

This thesis is intended to:

- Compare the fuel consumption of heavy duty trucks with and without e-dolly technology over the same distribution task.
- Compare the performance of heavy duty trucks with and without e-dolly on gradeability, vehicle average speed and number of gear-shifts.
- Verify how power split decisions are affected when lateral stability constraints are included in the control algorithm.
- Propose and assess a constraint that evaluates longitudinal stresses on drawbar coupling.

Limitations:

- The cost function J only takes into account fuel consumption, i.e. pollutant emissions, total energy consumption, battery degradation and transport time are not weighted in the equation.
- The combustion engine cannot charge the batteries, i.e. road charging is not considered.
- The target State of Charge (SOC) curve is based on linear and piece-wise linear functions with respect to distance, i.e. global optimum solutions are not found in the EMS.
- Longitudinal load transfer is not considered, i.e. distribution of vertical load between axles is constant.
- A single-track model with linear lateral tyre models is applied to assess vehicle lateral dynamics.
- Coulomb friction is assumed between tyre and road contact surfaces.
- Friction brake distribution is proportional to axles' vertical load.

1.5 Outline

This document follows the subsequent order. Chapter 2 describes the OC, it's properties and how some of them were acquired. In chapter 3, vehicle's powertrain models are described and a detailed explanation of the control strategy is shown. Next, in chapter 4, the lateral dynamics model applied in Dymola is stated and the grip margin expression derived. Chapter 5 demonstrates some plots from the simulations using the models derived in the previous chapters. After model validation, all results (relative to goals) will be displayed along with general comments on the outputs. At the end, in chapters 7 and 8, a conclusion will be exposed and future works will be exhibited.

2 Transport Mission

The operating cycle represents a distribution task performed by heavy duty trucks in Sweden. The goal is to transport goods between the cities of Gothenburg and Borås, which might also be referred as port and dry-port from now on. The mission begins at the port in Gothenburg and goes to the dry-port at Borås, where freight is unloaded and battery charges can be made. The truck is then loaded and driven back to the port. The task described represents one cycle and it has a total extent of 152 kilometres.



Figure 2.1: *Operating cycle view from GPS. Font: Geocontext.*

Mission properties are described using the Operating Cycle format [7]. The OC gives a numeric description of a transport task so that it can be standardized and applied into simulations. The format describes any mission with four domains, they are: the Road, responsible to store route legal speed and topography data, for instance; Weather, like surrounding temperature and ambient pressure; Traffic, to point the position of traffic lights in the road; and the Mission, that states where the vehicle should stop, recharge, load/unload, etc.

All the information stored in the OC structure is used by the Operating Cycle Block in Simulink (1.3) to give knowledge of the surroundings to the Driver, representing a visual view of the environment so that the driver can perform acceleration or brake decisions. For further information, the reader must refer to [7] that broadly describes the format and how to apply it in simulations.

To provide data in the OC structure, some mission parameters, e.g. the road curvature, were acquired using free on-line tools. Internal Volvo data was also applied in the format. The tool for getting road curvature allow users to sketch circles over a map and get their radius in the desired units. It was obtained for the most critical parts of the circuit.

3 Vehicle Longitudinal Model

The modelling approach used to describe the longitudinal dynamics of the LCV is grounded on [8]. In the referenced report, strategies assumed in this thesis to design transmissions, engine, pedals and chassis using physical expressions and Simulink blocks, are explained. However, these models can only represent a conventional diesel truck. In order to depict the hybrid topology, additional models are needed, such as the control unit, the Electric Machine (EM) and the energy storage system. This chapter focus on describing the modelling of these extra features in HEVs, except for the EM that can be modelled similarly to the engine. But before exposing them, a short elucidation of the longitudinal simulation process is provided next.

The brake and accelerator pedals are used as inputs to the vehicle model. Based on their displacement from standstill (D_{acc}, D_{brk}) the driver's power demand is estimated using a linear pedal map (Eq. 3.1). Positive values are given to acceleration and negative for deceleration demands.

$$P_{dem} \ = \ P_{dem}(D_{acc} \ , \ D_{brk}) \tag{3.1}$$

Fixed P_{dem}, it is used to feed the control unit so that the power split decision is taken. Then, each machine (ICE and/or EM) transmits power to the wheels via the transmission system. The gearboxes rely on the vehicle speed to perform gear-shifts, and thus selecting the proper gear ratio (i). The path efficiencies, e.g. from the differentials and gearbox, are accounted as gains in the Simulink model. At last, the wheels' propelling (F_{prop}) and brake (F_{brk}) forces are summarized with the road slope, the aerodynamic and rolling resistances (F_{res}) and divided by the vehicle mass (m_v) to compute the truck's longitudinal acceleration (a_x), which is then integrated to find the longitudinal speed (v_x). This process repeats until the trip ends.

$$a_x \ = \frac{F_{prop} \ - F_{brk} \ - F_{res}}{m_v} \tag{3.2}$$

3.1 Energy Storage System

Nowadays, most electrified vehicles use energy storage systems, such as lead-acid and Lithium-ion batteries, to store and manage electric power on demand. As shown in the report published by McKinsey & Company [9], this scenario has become possible due to technological advances provided by the car industry, which has made strides towards profitability and energy storage capacity of batteries in the past few years. Other technical improvements also have a major impact on the profitable production of electric vehicles. Better energy-to-mass ratio, slow self-discharge (while the device is not in use), fast charging and high energy efficiency made battery and electricity more attractive in vehicle application than other renewable energies, e.g. hydrogen fuel cells, that were gathering ground in the industry.

The challenge of an engineer is to select the best battery type given the costumer's needs, since the vehicle acceleration capability, driving long distances, and decreasing cost of ownership depend on the battery characteristics. It can possess high specific power or energy capacity, which influences the vehicle acceleration and electric range, respectively. There are some aspects that must be taken into account while choosing batteries for a propulsion system. They are for instance, usual range (km) covered by the vehicle, acceleration request and start-stop conditions presented in the operation cycle. The latter case is frequently seen in public transportation tasks, which encourages the application of hybrid and full electric vehicles. In order to identify how the battery type affects the truck's capabilities, a pre-selected set of batteries was applied and compared in the simulations. Table A.1 holds the technical specification of the batteries implemented in this work.

Traditional batteries carry a dependence on temperature that might cause drastic drops on their performance and cycle lifetime. Temperature fluctuations may be caused by internal chemical reactions or eventual climate changes, possible to occur during long haul driving. The problem exposed requires enhanced models to describe the side-effects of temperature on battery properties, which in turn demands heavy computational power and parametrization methods. To avoid complex modelling of the ESS, it is assumed that the vehicle has a cooling system that keeps the device at room temperature (around 27°C), thus, thermal effects on battery states can be neglected.

3.1.1 State of Charge

Battery state of charge must be monitored with precision in order to allow reasonable power split decisions by the controller. Several estimation techniques are presented and discussed in the literature, interested readers are referred to [10]. The SOC tracking strategy of this powertrain is inspired by the Coulomb, or Ampere hour, counting technique. It is classified as an integration method whose main advantage relies on the low computational time and main disadvantage, the cumulative error given by the integral function. Following the Coulomb's idea, the actual SOC ($SOC(t)$) is expressed as the difference between the initial and used battery's charge as shown in equation 3.3. The second term of the expression represents the used charge, which is the ratio between the cumulated discharge and initial charge.

$$SOC(t) = SOC(t_i) - \frac{1}{C} \cdot \int_{t_i}^{t} \frac{P_{batt}(t) \cdot dt}{V(t)} \tag{3.3}$$

According to [10], any integration method used to track the battery's SOC will become unreliable after a long period of time due to the cumulative error inherit to any integral function. This error might debilitate the controller's performance as it needs a correct reading of the SOC to perform the power split decisions. Also, it is informed that the method's accuracy is dependent on the knowledge of the initial SOC. From a simulation perspective, this requirement is effectively fulfilled, since $SOC(t_i)$ is a pre-defined parameter. Concerning the cumulative error, for a Plug-in HEV, the integral can be often reset, i.e. set to zero, since one can assume that the battery is fully charged at the beginning of each cycle, avoiding the cumulative error.

In the previous equation, P_{batt} is the input or output battery power (W), V is the battery's open circuit voltage (V) and C is the battery capacity (C). The integration, from the initial condition t_i until an instant of time t, is applied to compute the battery's used capacity due to the electric power usage.

A characteristic of chemical batteries is that the terminal voltage is directly dependent on the actual state of charge. Observing Fig. 3.1, one can understand this relationship and assume that the best utilization range of the storage unit is between 20 and 90 %, where the output voltage remains relatively constant.

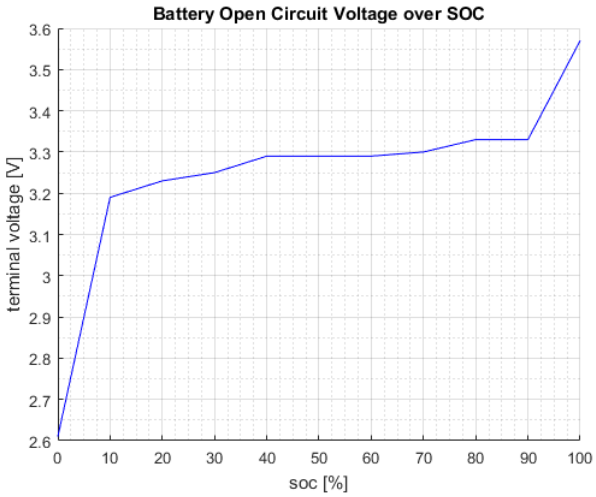


Figure 3.1: *Open Circuit Voltage (OCV) curve of a new battery cell. The reader must refer to [11] for further information. Data from Volvo Group (modified).*

Reported the SOC estimation technique, a second state and its measurement approach will be described in the next section.

3.1.2 State of Health

Any battery is subjected to degradation by calendar or cycle aging factors [11], these properties will influence the energy storage capacity of the cells and consequently the available electric power of the hybrid vehicle. When degradation reaches a critical threshold, the battery must be replaced to preserve vehicle's performance, however, this replacement generates additional costs to the owner and environmental issues (disposal of unhealthy units). Usually, for EV, HEV and PHEVs the end-of-life of a pack is reached when its capacity drops to 80% or its

internal resistance doubles compared to the manufacturer's specification [13]. To track the battery health, a variable that expresses the actual storage capacity in comparison to a brand new pack is used in the monitoring system, it's called State of Health (SOH) and is often given in percentage units. This variable aids the designer to choose a product that fits the costumer's needs, avoiding loose of electric propulsion, frequent recharges and short life span.

The battery degradation model is a curve fitting function dependent on, for instance, the number of cycles (N_{cycle}), and is represented in this work as follows:

$$\Delta SOH = \frac{P_{cell}}{f(N_{cycle})} \tag{3.4}$$

Where,

$$\Delta SOH = \int \frac{d(SOH)}{dt} \cdot dt \tag{3.5}$$

3.2 Energy Management Strategy

As stated in the previous chapters, any hybrid vehicle must have an Energy Management Strategy to take the power split decisions. The strategies used to perform the energy control are divided into two main areas, real-time (instantaneous) and off-line (predictive) control. The latter method relies upon previous knowledge of the Operating Cycle (e.g. topography), vehicle hardware (e.g. engine and electric machine) and on representative models of them. Applying optimization algorithms, global optimum control decisions can be acquired at a cost of high computational power and time. To apply this method in real-time situations the problem must be represented in a convex form, e.g. one must express the ICE and EM power characteristics with polynomial equations. The drawback of representing machines' behaviour with low order polynomial equations is that one might lose representativeness of the machines' true performance, thus this approach was not applied in this thesis. On the other hand, instantaneous methods are generally based on heuristic rules and the optimal strategy is highly dependent on the developer's expertise. It disregards most of the road properties and generally takes into account powertrain specifications. Therefore, this approach has fast computation, allowing on-time implementation, but losing optimality.

The control applied in this framework is the Equivalent Consumption Minimization Strategy (ECMS), an instantaneous approach. Unlike most heuristic methods, the ECMS relies on optimization algorithms, however it reduces the global minimization problem (Eq. 1.1) to an instantaneous one that can be quickly solved and implemented in on-line events [14]. This approach applies a proportionality factor to the cost of electric power compared to the cost of fuel power, thus an equivalent fuel consumption can be associated with the use of electricity from the batteries. The ECMS optimality depends on the magnitude of this equivalence factor (λ) that might change during a transport task. Normally, an optimum set of λ is found using optimization algorithms. Then, it is stored and used as a look-up table by the control unit to solve the optimal control problem. However, in this thesis, an adaptive ECMS method will be applied. This approach does not require the pre-computation of any set. The following subsections will describe in detail how the controller makes power split decisions in the powertrain based on this methodology.

3.2.1 Objective Function

The ECMS objective function is not only a mathematical expression capable of rating the cost of a control action but also, if minimized, represents the optimal power split decision. The equation used in this thesis is presented in (3.6) and as it can be observed, this function is not an integral of time, but rather a straight-forward (instantaneous) function. From the expression, the engine power (P_{eng}) is a function of the mass flow rate ($\dot{m}_f$) and lower heating value (Q_{lhv}) of the fuel, in this case, the diesel. Concerning the battery power (P_{batt}), the actual energy consumed from the cells is given by the output power at the terminals (P_{out}) and the internal losses due to chemical reactions ($P_{chemical}$). The equivalence factor (λ) acts as a penalty function, designed for a specific transport task, and will be treated separately in section 3.2.4. As discussed, this method does not provide global optimum solutions, but rather an instantaneous one.

$$J = P_{eng} + \lambda \cdot P_{batt} \tag{3.6}$$

Where,

$$P_{eng} \;=\; P_{eng}\,(\,\dot{m}_f\;,\;Q_{lhv}\,)$$

$$P_{batt} \;=\; P_{batt}\,(\,P_{out}\;,\;P_{chemical}\,)$$

In the optimization problem, the battery output power is taken as the design variable. For each iteration a guess value must be assigned to P_{out} and the chemical losses, the engine power and the final cost must be computed.

3.2.2 Optimization Framework

The block diagram shown in Fig. 3.2 represents the optimization framework used by the control system to perform the power split decisions. The input signals are related to the current vehicle states, such as longitudinal speed and battery SOC, and the driver's power demand, translated via position of throttle and brake pedals. After executing the optimization process, the control unit must return a set of signals that states how much power each device must supply in order to meet the driver's demand. In the following lines a brief description of the optimization process is provided. The interested reader shall find further information of optimization methods in [15].

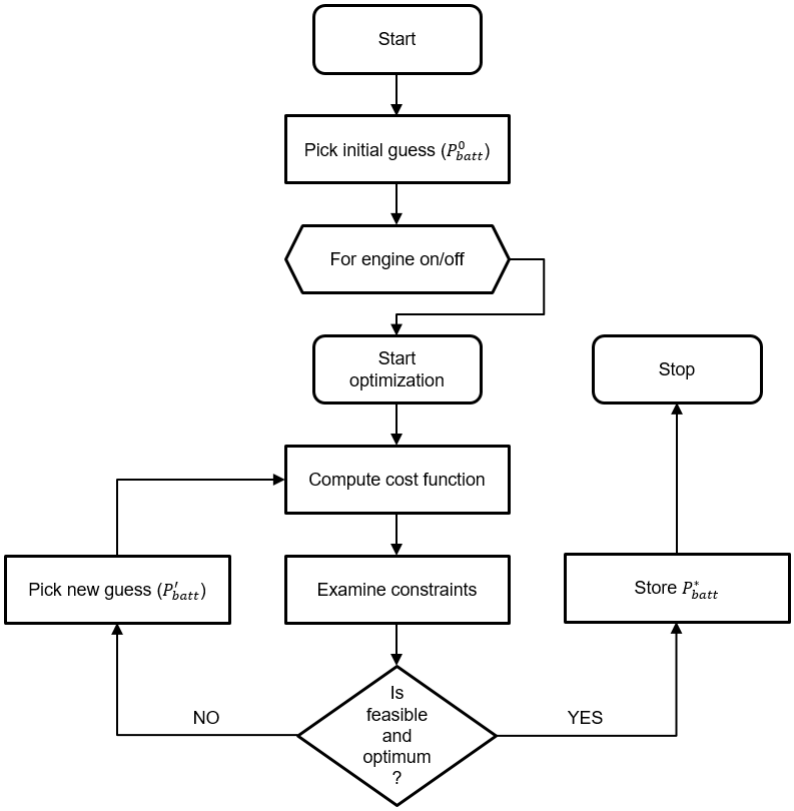


Figure 3.2: *Flowchart representing the optimization framework used to perform the control unit power split decision.*

The optimization algorithm is initialized after specifying a preliminary guess, P^0_{batt}, which can be, for instance, the power demanded by the driver. P^0_{batt} is used in the first of many iterations required to solve the instantaneous minimization problem. In each iteration the algorithm tries a different guess and both P'_{eng} and P'_{disc} (power delivered by the brake discs) are found by solving a linear system of equations. Here, the prime super-index stands for iteration. The following section describes how they are estimated from P_{dem} and P'_{batt}. Given the iteration variables, P'_{batt} and P'_{eng}, the cost function is calculated and the constraints verified. If the proposed solution is feasible and optimum, it is stored. This process is carried out until the algorithm's criterion for optimality is satisfied, i.e. the cost is a global minimum for the studied instant of time, or until the process reaches a limit, e.g. time allowed for optimization. The control unit will then pick the stored action P'_{batt}, now designated as the optimal control action (P^*_{batt}), compute P^*_{eng} and P^*_{disc}, and send the signals to their respective devices.

Power-train Dynamics

For trucks powered with electrified dolly, the driver's power demand must be supplied by the batteries, brake discs or engine. This relation is displayed in Eq. 3.7.

$$P_{dem} = P_{batt} + P_{disc} + P_{eng} \tag{3.7}$$

The ECMS objective function presented in Eq. 3.6 requires previous knowledge of the battery and engine output power. Whenever the driver desires to propel the vehicle (i.e. positive power demand) the system assumes that the brake discs must stay unapplied ($P_{disc} = 0$). Since both P'_{batt} and P_{dem} are known, P'_{eng} can be estimated by solving a system of equations that contains, for example, Eq. 3.7.

Regarding deceleration scenarios the following remarks can be made to explain how the optimization framework finds a solution. It is known that both ICE and brake discs convert power into not useful heat. In order to make better usage of the truck's kinetic energy, the system will prioritize braking with the electric drive so that the batteries are recharged using EM's generator functionality. The amount of electric energy recovered and thus brake is often bounded by either the battery or electric machine capabilities, e.g. maximum power that the battery or EM can receive. Beyond this limit, the remaining power demand must be supplied by other systems, prioritizing the engine and then the brake discs. However, the ICE will only participate in braking if it posses an exhaust brake utility. A schematic of the prioritization method is outlined in Fig. 3.3.



Figure 3.3: *Priority diagram for braking scenarios, high priority is given by the intensity of the red line. Sources: Meritor (brake), Volvo Trucks (engine) and [16] (electric machine).*

In this work, the e-dolly propelled axle receives all the brake energy that it can sustain. The limit is either from the electric drive (batteries and EM capabilities) or from the available road friction. If the EM reaches its full potential on power generation, or if the batteries are fully charged, and the tyre is not saturated in friction, the disc brake can be actuated on this same axle. Remaining deceleration demand, if it exists, is then distributed equally over the other axles. Here, the engine does not have an exhaust brake utility.

3.2.3 Constraints

An optimization algorithm can use constraints to guide the tool in the search for an optimal solution. In the hybrid control case, constraints are based in hardware and physical limitations. For example, the electric drive can only provide or receive a certain amount of power, this limitation can be translated into a constraint as demonstrated by Eq. 3.8. Furthermore, the e-drive capability is bounded by either the battery or electric machine, provided that the first could produce an amount of power that is larger than what the electric machine can endure and vice-versa. Not only that, but in the same manner as the maximum battery power (P^{max}_{batt}) relies on the number of packs and cells that it posses, the number of electric machines within the drive must also be contemplated while assessing the system limitations. Gathering these statements one can represent the maximum and minimum e-drive power as in 3.9 and 3.10, respectively.

$$P^{min}_{e.d.} \quad \leq \quad P_{e.d.}(t) \quad \leq \quad P^{max}_{e.d.} \tag{3.8}$$

Where,

$$P^{max}_{e.d.} = \min(\ P^{max}_{batt},\ P^{max}_{e.m.} \cdot n_{e.m.}\ ) \tag{3.9}$$

$$P^{min}_{e.d.} = \max(\ P^{min}_{batt},\ P^{min}_{e.m.} \cdot n_{e.m.}\ ) \tag{3.10}$$

Regarding the engine limits, a straightforward relation can be prescribed as follows,

$$P^{min}_{eng} \quad \leq \quad P_{eng}(t) \quad \leq \quad P^{max}_{eng} \tag{3.11}$$

Longitudinal stresses on the drawbar must never exceed the physical limit of the hardware. Constraint 3.12 ensures this limitation. The equation used to estimate $F_d(t)$ is derived from a longitudinal free-body diagram of the articulated vehicle and is shortly described in the appendix.

$$F_d(t) \quad \leq \quad F_d^{max} \tag{3.12}$$

Vehicle stability will be described by the available grip between tyre and ground. Whenever a split action, being evaluated by the controller, leads to a grip below the pre-defined threshold, this action will be disregarded from the optimization algorithm to avoid wheel slip. Therefore, the instantaneous grip margin, $\Delta_\mu(t)$, must stay within a safe zone through the entire cycle (3.13). The approach used to determine $\Delta_\mu(t)$ will be discussed later in section 4.2.

$$\Delta_\mu(t) \quad \geq \quad \Delta_\mu^{min} \tag{3.13}$$

The topology appraised in this work has no mechanical, neither electrical, link between the ICE and the EM. This way, battery recharge cannot be directly made by the engine. However, the system could choose to perform a strategy called *road charging*. To explain this strategy lets consider the following scenario. The driver demands an amount of power P_{dem} to propel the truck forwards. Then, the controller decides that the engine will provide more power than the one demanded ($P_{eng} > P_{dem}$). Performing a balance equation one will notice that an extra quantity of power (P_{extra}) is left on the system as follows.

$$P_{dem} - P_{eng} = P_{extra}$$

To balance this equation, the controller decides to also brake with the e-drive, thus recharging the batteries.

$$P_{dem} - P_{eng} + P_{e.d.} = P_{extra} = 0$$

This strategy is called *road charging*, as the connection between ICE and EM is given through the road. Not knowing the scenarios that could benefit from this strategy, as energy conversion usually involves losses, the *road charging* will be avoided applying the constraint expressed in Eq. 3.14. $\eta_{c.d.}$ is the path efficiency of the combustion drive, i.e. efficiency from the engine to the wheels.

$$P_{eng}(t) \ \cdot \ \eta_{c.d.}^{-1} \quad \leq \quad P_{dem}(t) \tag{3.14}$$

Any wheeled vehicle has its propelling/braking forces on axle 'i' (F_{i_x}) limited by two factors: the powertrain capabilities, or the road friction (μ) limit and respective axle load (F_{i_z}). This property is described in equation 3.15 and is based on [5].

$$F_{i_x} = \min(F_{i_{pwt}}; \mu \cdot F_{i_z}) \tag{3.15}$$

The powertrain forces ($F_{i_{pwt}}$) are dependent on the power delivered by the propulsion system ($P_{i_{prop}}$) at wheels, which includes all efficiencies along the path "motor to wheel", and the brake power ($P_{i_{disc}}$) provided by the brake discs, see equation 3.16. Also, the vehicle speed (v_x, m/s) and the rolling resistance (2$^{\text{nd}}$ component of the expression) are needed to properly compute the force acting on the tire. C_{RRC} is the rolling resistance coefficient.

$$F_{i_{pwt}} = \frac{(P_{i_{prop}} + P_{i_{disc}})}{v_x} - C_{RRC} \cdot F_{i_z} \tag{3.16}$$

For the current case study the propulsion power can be given by either the ICE or EM, assuming respective efficiencies, and is only present on the propelled axles. Therefore, an inequality constraint can be formulated (3.17).

$$F_{i_{pwt}} \leq \mu \cdot F_{i_z} \tag{3.17}$$

Other constraints are applied to secure the method feasibility and will not be covered in this report.

3.2.4 Determining the Equivalence Factor

In a nutshell, the equivalence factor (λ) states the worthiness of using electricity from the battery than using fuel from the tank. Therefore, if the value of λ is high, the algorithm will infer that the cost of using electrical power is expensive, i.e. the controller is encouraged to use the engine while being discouraged from using the electric machine to supply any power demand from the driver.

Usually, λ is defined as a map that points to its optimal value given the battery's state of charge and the vehicle position on the transport task. Optimization algorithms or machine learning methods, e.g. dynamic programming [17] and reinforcement learning [18], are commonly used methods to compute the optimal set. However, these approaches require high computational power, time and previous knowledge of the mission and vehicle architecture. As a consequence, the values must be pre-computed and stored, or initialized before starting the simulations. Also, the solution becomes very sensitive to the road and vehicle properties, i.e. a set might be only optimal for a particular scenario. Once the parameters have been defined, table look-up methods can be used to update the equivalence factor along the driving cycle, providing fast computation of the split decisions.

In this work, the equivalence factor is estimated using an adaptive control method, which considers the actual battery state of charge, function of time, and a target state of charge curve, function of the vehicle position relative to the cycle (Eq. 3.18).

$$\lambda(SOC_{actual}(t); SOC_{target}(x)) \tag{3.18}$$

This approach does not require pre-computation of any set, the magnitude of λ is given by the deviation of the actual SOC to the target one. The penalty function applied to estimate the equivalence factor is based on a tangent function [19]. The main advantage of the adaptive property is the flexibility given to the controller, which does not need to follow the target curve, but rather use it to guide the power split decisions.

While using ECMS, the target curve should represent the global optimal trajectory of the battery's SOC through the mission. In turns, the curve would provide the ideal way to use electrical energy from the storage unit. For instance, this curve could be found using optimization algorithms. Fig. 3.4 depicts a global optimum curve achieved using Dynamic Programming [20].

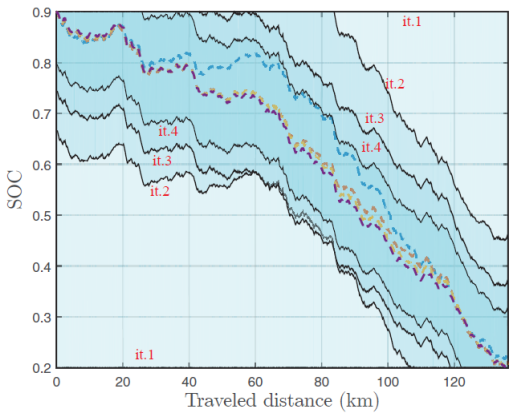


Figure 3.4: *Optimal SOC curves acquired using dynamic programming. "It" stands for iteration. Plot from [20].*

Still, this work must not seek for optimal target curves. Therefore, the following assumption was made. Examining the optimum curves was noticed a linear trend from the initial towards the final SOC. Taking advantage of this fact, linear and piece-wise linear functions were used to represent the target SOC (Fig. 3.5). It is clear that this assumption cannot lead to the best energy usage, but at least provide a satisfactory way to perform the control decisions. Each curve represents a different charging scenario. For the dashed one it is assumed that a charging station is available at the dry-port, so the batteries can be recharged while the freight is being unloaded off the trailers. As regards to the straight line no charging is performed during the cycle.

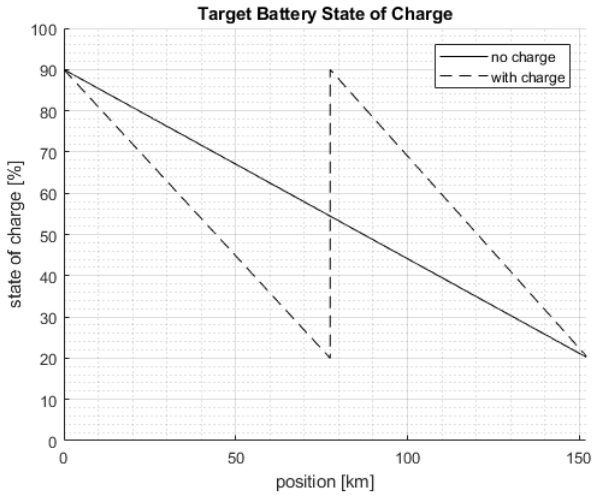


Figure 3.5: *Optimum state of charge target curves used in the simulations. The solid line represents a scenario without charge, and the second with it.*

The tangent function makes the ECMS feasible for online applications because the optimal SOC curve is only used to aid the control unit and must not be precisely followed. For example, to overtake another vehicle, the powertrain is highly requested for power. If the control unit was compelled to strictly follow the SOC reference, maybe, the driver would not have access to any other amount of power other than the one stated by the optimal SOC curve. With the tangent function, flexibility is given to the control method. Now, the optimal SOC curve can be disregarded and more power accessed by the controller. As a consequence, a penalty is applied to the cost of electric energy.

The figure below illustrates the tangential behaviour of the penalty function. If the actual charge deviates from the target (Eq. 3.19), causing the battery to have less stored energy than it should (positive deviation, $SOC_{dev} > 0$), the magnitude of λ must increase, indicating that the electricity cost is higher than the fuel. This is represented in the middle chart of Fig. 3.6. The opposite can be assumed if the battery has more energy than the target value and it is represented in the rightmost plot.

$$SOC_{dev} = \frac{SOC_{target} - SOC_{actual}}{SOC_{target}} \tag{3.19}$$

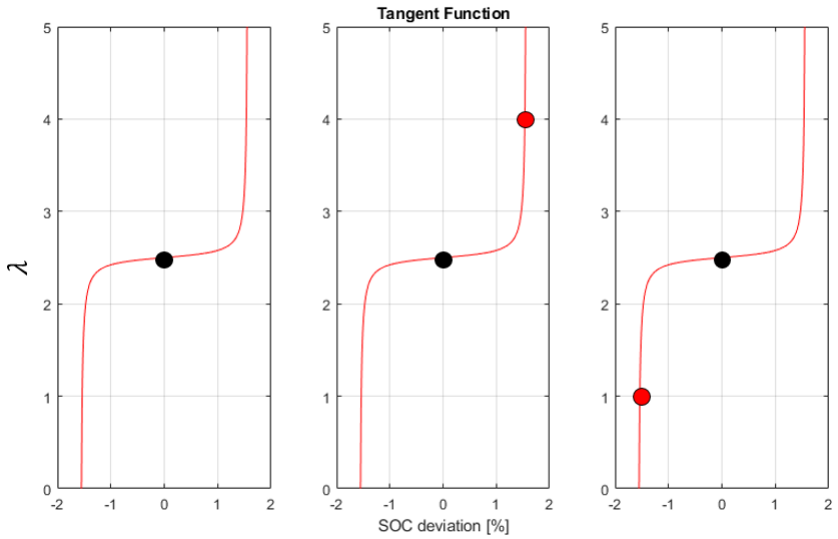


Figure 3.6: *Representative shape of the tangent function used by the control algorithm to penalize the equivalence factor due to deviations from the target state of charge.*

Described the longitudinal model, the next chapter will discuss the equations and methods applied to asses the A-double lateral dynamics and how it is assembled to the longitudinal frame.

4 Vehicle Lateral Model

Any commercial vehicle may be subject to roll or yaw instability while driving, but articulated vehicles in particular, e.g. long haul trucks, are more inclined to develop unpredictable behaviour than non-articulated vehicles (i.e cars). Factors that can give an explanation for this sensitiveness are high centre of gravity and one aspect native to articulated vehicles, rearward amplification. As specified by [21], yaw stability is mainly dependent on both vehicle speed and lateral acceleration.

As mentioned, combination trucks are more sensitive to lateral acceleration than regular vehicles, but hybrid trucks coupled with two separate propulsion systems might have greater tendency to be unstable. According to [5] a rolling tyre is much more laterally stiffer than propelled or braked ones. Therefore, the driven tyres of the e-dolly have less resistance to lateral disturbances and the vehicle must be less stable. On that account, to avoid scenarios where a combination of lateral and longitudinal acceleration produces saturation of tyre's side or frontal grip, leading to spinout, jackknife or trailer swing, a simulation block must be implemented in the longitudinal model to constraint tyre saturation level while optimizing the torque split.

4.1 Vectorized model

The lateral stability model applied in the main simulation framework is a vectorized single-track model for articulated vehicles that uses Modelica language to be described [22]. The one-track hypothesis implies that tires belonging to the same axle are treated as a single virtual tire, positioned at the centre of the holding axle, which simplifies equations and improve simulation speed without losing relevant reliability. Modelica coding style does not require explicit formulation neither to use symbolic toolboxes in order to find results from a system of equations, the compiler is responsible to perform all necessary mathematical actions to solve the problem, preserving the intuitive shape of all expressions. Furthermore, the coupling equations were held as non-linear kinematic constraints, avoiding small angle approximation between units and validating the model for high/low-speed manoeuvres.

The combination truck considered in this research possess 4 units, 5 group of axles and 11 axles. Only the first axle of the tractor is steered, i.e. the e-dolly is modelled without a steerable axle. The second axle of the tractor and e-dolly units is propelled; by an ICE and an EM, respectively. The system of equations that describes the dynamic behaviour of the truck is also described in [22] and are designed to represent a large range of articulated vehicles. Thus, to make use of this tool, one must supply the model with arguments that define the truck's shape, e.g. number of units, axles, metric dimensions and tire properties. The A-double 6x4 was defined using *OpenPBS* library [23].

In order to match the Modelica lateral model with the Simulink longitudinal model, so co-simulation became possible, a modification on the longitudinal force balance equation on the Modelica model was made. Comparing Eq. 4.2 with the one presented in [22], Eq. 4.1, it is possible to notice that this expression has additional elements. Air drag and road grade contributions were the changes implemented in this equation, essential elements to evaluate vehicle longitudinal performance. The air drag resistance depends on the drag coefficient (C_{drag}), the air density (ρ_{air}) and vehicle frontal area (A_{front}), while the road grade contribution is a function of the gravity acceleration (g), the road grade (φ) and vehicle mass (m). Even though this modification was applied, to compute the same vehicle states from both environments is difficult, since different solvers and techniques are used within each platform, thus the results from each approach might have a small divergence.

$$m \cdot a_x = F_x - F_{c_{x,rear}} + F_{c_{x,front}} \cdot \cos\theta - F_{c_{y,front}} \cdot \sin\theta \tag{4.1}$$

$$m \cdot a_x = F_x - F_{c_{x,rear}} + F_{c_{x,front}} \cdot \cos\theta - F_{c_{y,front}} \cdot \sin\theta - 0.5 \cdot C_{drag} \cdot \rho_{air} \cdot A_{front} \cdot v_x^2 + m \cdot g \cdot \sin\varphi \tag{4.2}$$

Having fixed the vehicle of interest and given the appropriate inputs, here defined as tire steering angle (δ), longitudinal forces on the axles (F_x) and road slope, the system is able to determine the vehicle speeds (v_x, v_y and ω_z), accelerations (a_x, a_y and $\dot{\omega}_z$) and remaining unknowns, e.g. lateral forces on the wheels (F_y) and tire side slip (s_y). These variables are used to compute the tyre's grip margin, discussed in the following section.

4.2 Strategy for Vehicle Stability Analysis

Any wheel rolling on a rough surface has its maximum traction/brake force, F_w, bounded by the road coefficient of friction (μ) and by its normal load (F_{w_z}) as described in equation 4.3. This assumption gives a bases for the friction circle theory, which represents the relationship between tire and road surface.

$$|F_w| = \sqrt{F_{w_x}^2 + F_{w_y}^2} \leqslant \mu \cdot F_{w_z} \tag{4.3}$$

The theory states that, the norm of any vector acting on a wheel lies within a circle of radius $\mu \cdot F_{w_z}$. A graphical representation is shown in Fig. 4.1. From the diagram, one can identify the tyre, which rolls over the xy plane (ground), the disturbing force F_w and its lateral (y) and longitudinal (x) components, and the friction circle with radius R, function of the proposed parameters. Also, one must notice that both circle and vector have origin at the centre of the wheel contact patch, considered uniformly distributed over the ground.

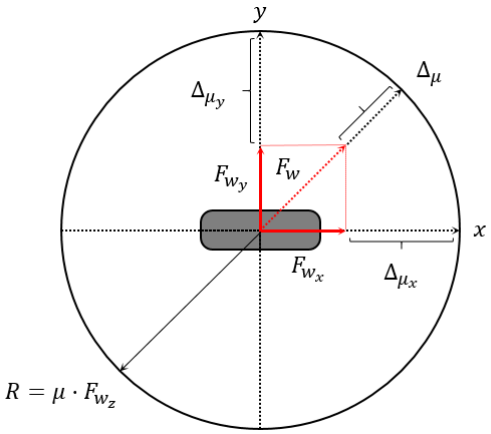


Figure 4.1: *Graphical representation of the friction circle applied to rubber tyres.*

The strategy for stability analysis takes the difference between friction limit and applied force, here addressed as margin grip (Δ_μ), to inform that the vehicle is stable or not. As shown in Eq. 4.4 the margin is a normalized variable. Therefore, a vehicle will be considered stable if the margin stays within the 0 and 1 range, implying that the tire is not sliding front or sideways (stable behaviour). By analogy, if the margin goes below zero, one can assume that the tire is slipping and that the normalized force has magnitude greater than one, exceeding friction circle radius. The normalized friction circle is illustrated in Fig. 4.2.

$$\Delta_\mu = \frac{\mu \cdot F_{w_z} - \sqrt{F_{w_x}^2 + F_{w_y}^2}}{\mu \cdot F_{w_z}} \tag{4.4}$$

In section 1.4, it was mentioned that a linear tyre model is used in the vectorized model, i.e. it assumes no friction saturation. Considering that a brush tyre model with combined slip and uniform pressure distribution remains linear until half of the tyre's maximum longitudinal force ($|F_{w_x}| = \mu \cdot F_{w_z}$) [5], it is possible to assume that the linear model is valid until the same measurement. Therefore, instability must be addressed if Δ_μ goes below a 0.5 threshold. Observing this approach, one cannot state what kind of instability event the vehicle is experiencing but only infer that the wheel is slipping. Then, using Δ_μ information, the control unit must take actions, if necessary, to avoid tyre slip, for example, by choosing different power split or, in a more sophisticated control, delivering less power than the one demanded so friction saturation is not reached.

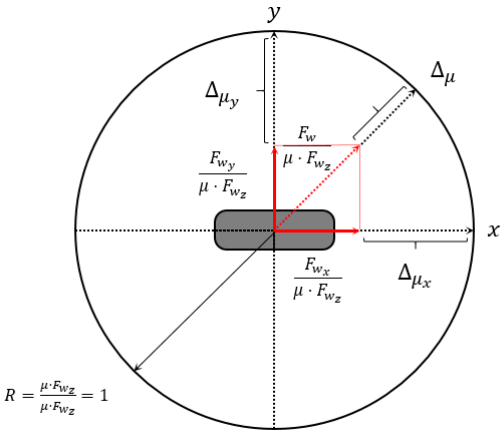


Figure 4.2: *Graphical representation of the normalized friction circle applied to rubber tyres.*

4.3 Implementation of the FMU

In automotive engineering, as the name suggests, longitudinal simulations are mainly concerned with describing the longitudinal vehicle dynamics. They are often used to asses, for instance, control strategies and the vehicle's energy consumption. In order to understand how the lack of lateral dynamics affects these simulations and their results, a FMU is used to include the vehicle's lateral dynamics into the longitudinal simulation model. The FMU, which was generated from the Modelica code, can be imported into Simulink as a block, or into Matlab scripts as a function. Both implementation methods were used in this thesis.

The first one was applied to observe how many critical events are found in the studied cycle, i.e. how frequently Δ_μ of any tyre stays below the threshold. This FMU block substitutes the chassis block within the vehicle module, whose responsibility is to compute the vehicle longitudinal speed (v_x).

In order to compute the vehicle states and the margin grip, the FMU must be supplied with the tractive or braking forces on each axle, the road angle and the wheel steering angle. These inputs are provided to the block in the following manner. After computing the power split a simple logic is used to estimate the longitudinal forces acting over each axle. Power derived from, or going to (brake), the battery is applied in the propelled axle of the e-dolly. Power derived from the combustion engine is applied in the propelled axle of the tractor unit. Additionally, when it comes to braking, besides the power supplied by the resistive forces from the generator and rolling resistance, remaining brake energy is equally distributed among the other axles via brake discs. Forces are derived from Eq. 4.5.

$$F_{i_x} = \frac{P_i}{v_x} \tag{4.5}$$

The forces are then stored in a matrix and used as inputs to the FMU. It uses the equations presented in the previous section and computes all remaining unknowns, including the margin grip. The wheel steering angle is acquired as shown in Eq. 4.6, where L_{wb} stands for the length of the tractor's wheel base and c, the curvature.

$$\delta = L_{wb} \cdot c \tag{4.6}$$

The second approach, FMU as a function, was used to implement the instantaneous evaluation of Δ_μ within the optimization process. This way, the control unit can disregard any split action that leads to instability while solving the optimal control problem. The FMU is imported into the script using Modelon's Functional Mock-up Interface (FMI) Toolbox. When evaluating the margin grip Eq. 3.13 is used as a constraint. The FMU is called to compute all tyres margin grip, the lowest Δ_μ is stored and informed to the constraint. If this value is greater than the threshold, it is a valid split action. Unfortunately, this method requires to much computational time; therefore, a full simulation of the operating cycle was not performed but rather small sections of it.

5 Model Validation

In this section, the models and methods presented have been validated in order to ensure their reliability and consistency. Validation has been performed through analysis of the simulations' output, displayed in diagrams, and by a brief discussion on their behaviour relative to prior expectations. Such study will guarantee that reasonable answers are given to the thesis inquires.

State of charge tracking

Considering the adaptive approach imposed to the energy management strategy (described in section 3.2), it is expected that the actual SOC will have a similar shape to the target curve. Plotting the actual and target SOCs over the vehicle position (Fig. 5.1) it is possible to recognize that the battery level follows the presumption, remaining close to the reference. The latter characteristic confirms the flexibility given by the tangent function on the controller. One can also identify that the electrical charge, supposed to take place at the dry-port, was accomplished.

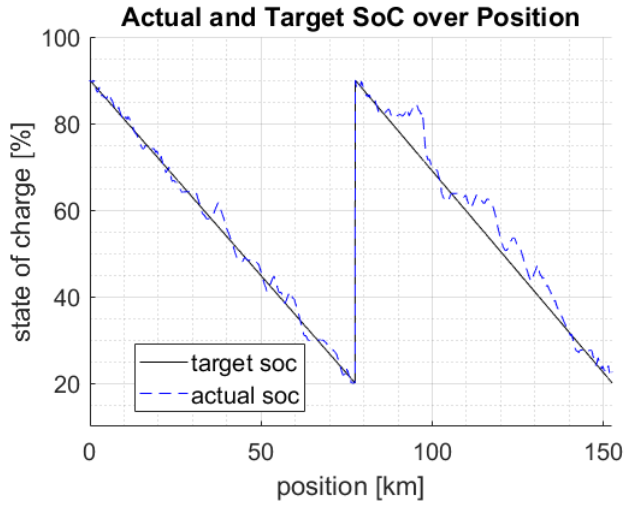


Figure 5.1: *Battery energy usage along the cycle. The blue line, true state of charge of the ESS, follows the black one, the target curve. The initial SOC is set to 90% and the final to 20%. Battery is recharged in the dry-port. Data from a 80 tonnes vehicle powered with D13 engine and three packs of energy optimized batteries.*

To further understand how the equivalence factor varies according to the actual charge state, λ was plotted over a small section of the cycle. Fig. 5.2 depicts the selected area. From the plot, one might identify that penalization is quickly given to λ whenever the SOC level diverges from the target and that the penalty applied to the equivalence factor is proportional to the deviation size. Initially, the battery level is below the reference, and therefore λ shows a high value. As the system recovers energy, the factor is penalized and its magnitude decreases, reducing the cost of electric power and stimulating the controller to consume electricity instead of fuel. The opposite can be noticed when the charge level ascends the target and the algorithm increases the cost of electricity, avoiding its usage. This behaviour is exhibited by the equivalence factor several times during the mission.

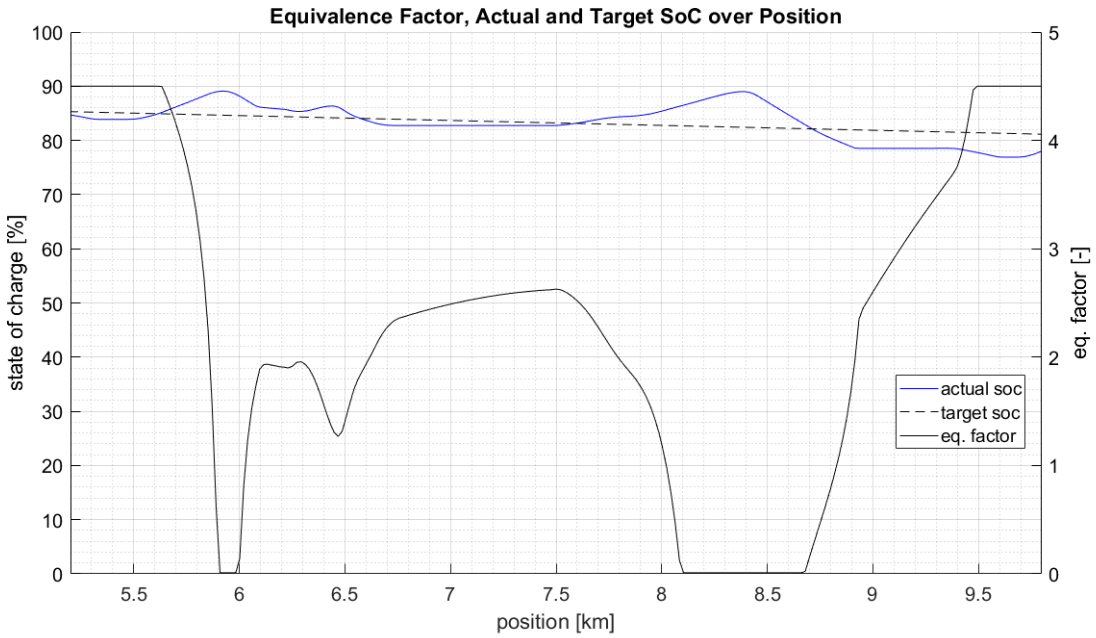


Figure 5.2: *Effects of the actual state of charge on the equivalence factor.*

Influence of road grade on vehicle speed

Assuming that propelling forces are kept constant, any vehicle subjected to a steep road grade will have its speed reduced due to gravity and increased if exposed to a deep grade. To make a sanity check of the proposed model, the following diagram of v_x and road grade over position is presented. One can visualize the changes in vehicle longitudinal speed due to road grade fluctuations. For example, as shown in km 62, a great amount of velocity is lost when the truck needs to climb a small hill, which is a common behaviour for heavy duty trucks.

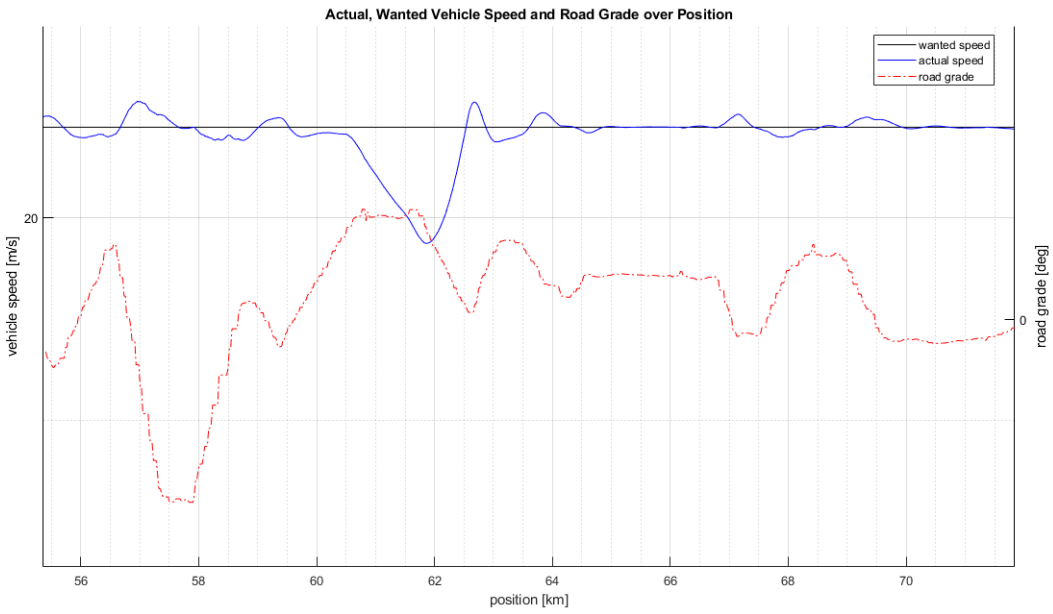


Figure 5.3: *The influence of road grade on the vehicle speed.*

Power distribution

The control approach, used to manage the energy flow within the system, must decide which machine will deliver the driver's power demand based on the equivalence factor. At some point, the cost of electricity will be lower than the fuel, under this circumstance the controller must use the electric drive to aid the engine, or even alone, to boost the vehicle. It must be done so the engine operates at a high efficiency zone and fuel can be saved. Furthermore, in the case of high equivalence factor, the ICE shall provide most of the demanded power, as the cost of fuel will be lower than of the electricity. Fig. 5.4 shows the power distribution of the powertrain in a section of the operating cycle.

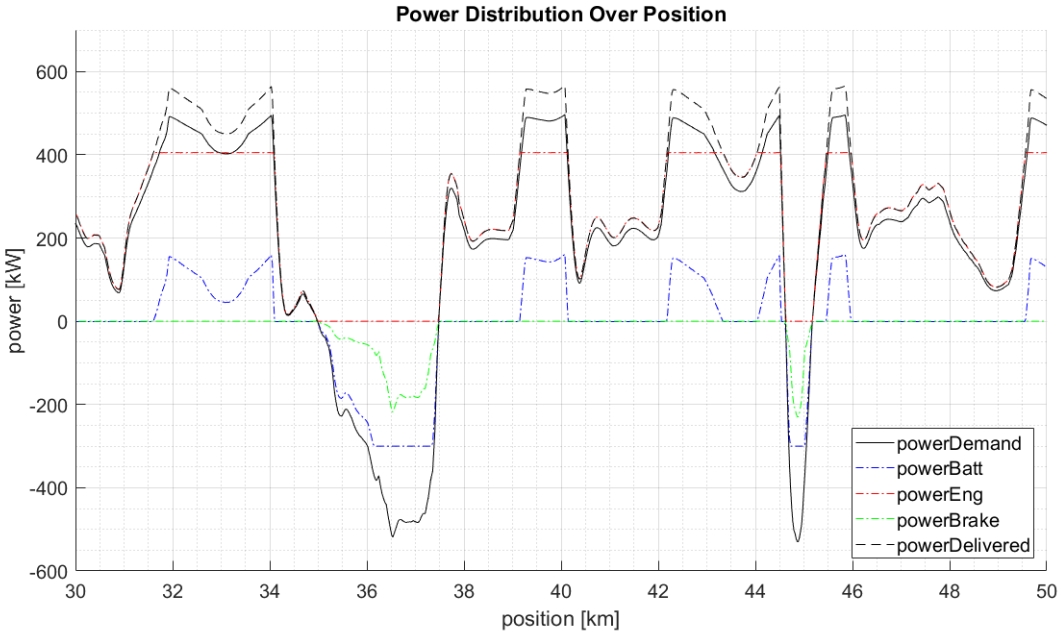


Figure 5.4: *Split actions performed by the control algorithm.*

From the diagram, one can verify that the electric machine, engine and brake discs add to each other in order to fulfil the power demands made by the driver. Moreover, the ICE is responsible to deliver the most part of the propelling power. With respect to braking scenarios, the EM is prioritized and the discs are used to complement the request. No engine brake can be observed in the plot due to the lack of exhaust brake functionality assumed in this system.

One can also notice that, while propelling the vehicle, the power delivered is always greater than the one requested, since every mechanical device that transport or converts energy holds an efficiency in its path that will reduce the output power (coming out from the machine) when compared to the input. In a powertrain this is given, for instance, by clutches, gears and differentials. During brake, this behaviour does not happen since friction brakes are considered ideal machines whose purpose is to convert energy into heat.

6 Results and Discussion

In this chapter, studies on vehicle performance and stability will be carried out using the simulation framework earlier defined. The objects of study, as stated, are two long vehicles (A-doubles) that differ by their Gross Combination Weight (GCW) and hardware. Some results will be displayed as percentages to cover sensitive data.

6.1 A Comparison on Fuel Consumption

For the same GCW, a truck may vary in engine size and battery type. Remaining machines, e.g. electric motor and gearbox, are fixed. Three engine sizes and six battery types are available for testing, further technical specifications are provided in the appendix (Tab. A.1 and A.3). Defined the design parameters, specific hybrid set-ups were compared to a regular diesel-powered truck in terms of mission fuel consumption. This comparison aims to understand which type of battery pack would perform best in the given powertrain considering price, electric range and fuel consumption.

Energy optimized batteries have larger storage capacity, but less throughput power, i.e. traction capacity. On the other hand, those power optimized have higher throughput power, but less storage capacity. So, the designer must make a trade-off between this characteristics and choose the product that best suits the costumer's needs. Normally, HEVs spend less fuel due to their extra electric motor. In this regard, it is expected from the following analysis that all combinations exhibit some fuel economy relative to the diesel-powered vehicle. Furthermore, the savings must be proportional to the battery's capacity, as the vehicle will have more access to electric power while performing the distribution task.

Starting with the 80 tonnes case, simulations were performed considering the load distribution from *OpenPBS* database (Tab. A.2 in the appendix). Later, total fuel consumption was stored for each combination under evaluation. Fig. 6.1 depicts the fuel saving of the hybrid topology in comparison to the conventional one for different battery types.

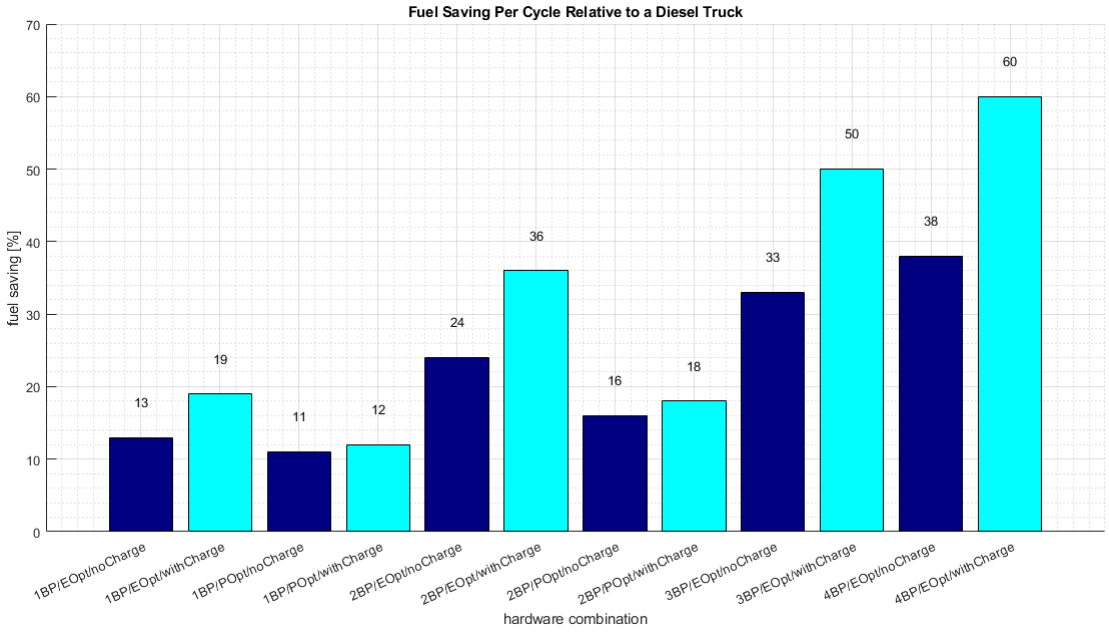


Figure 6.1: *Fuel saving of 80 tons heavy-duty trucks powered with e-dolly and D13 engine relative to a conventional diesel truck powered with a D16 engine. Nomenclature: BP - Battery Pack; E - Energy; Opt - Optimized; P - Power. withCharge and noCharge designates if the battery is charged or not at Borås.*

Based on the results, shown in the bar plot, it is possible to infer that the expected behaviour of fuel economy is present in all cases. Furthermore, the vehicle savings are proportional to the battery energy storage

capacity and to the presence of a charging station at the dry port. The last vehicle configuration, with four packs of energy optimized batteries, shows the best fuel saving, driving the majority part of the task in electric mode. Despite the significant fuel saving shown by this combination, the additional cost associated to its usage is much more expensive than a vehicle, for example, with 2 power optimized batteries. Therefore, the cost of ownership for this arrangement increases considerably, making it infeasible for the studied transport tasks. Considering the cost, fuel saving and the electric range, a powertrain equipped with two power optimized batteries shows the best cost-benefit ratio.

Fig. 6.2 shows the fuel savings for the 60 tonnes case. Compared to the previous results, similar statements can be made to this scenario. However, energy optimized batteries stand out over the power optimized ones, proving similar fuel consumption with a lower number o battery packs. This might be occurring because energy capacity is more relevant than traction capacity for this lower weight case, i.e. the truck does not required all the traction power provided by the power optimized models.

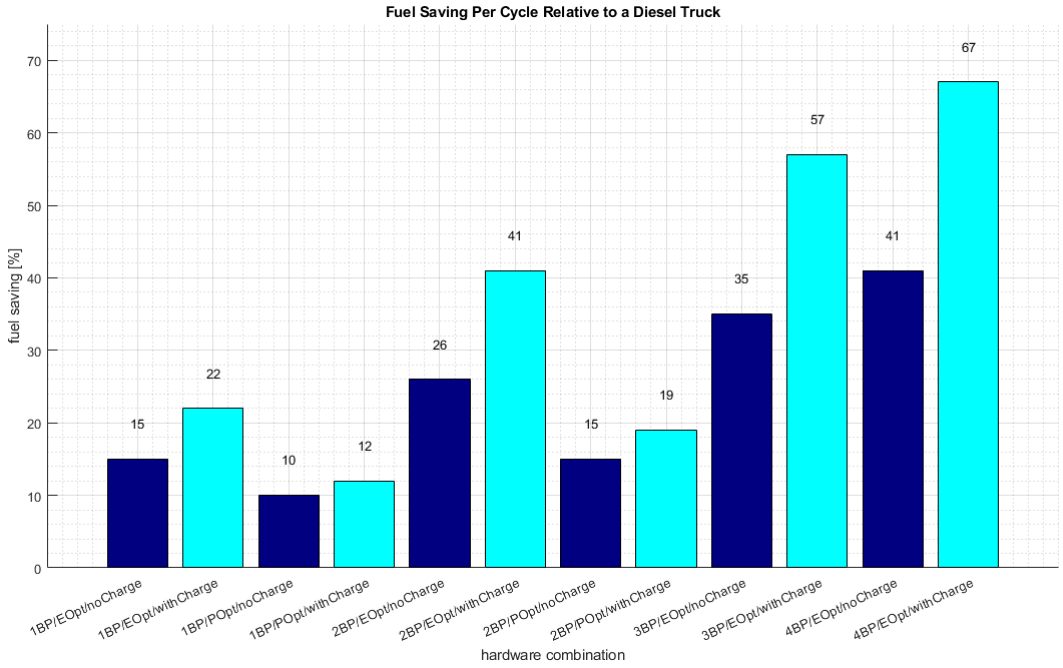


Figure 6.2: *Comparative analysis of different hardware combinations for a 60 tons heavy duty truck.*

6.2 A Comparison on Vehicle Performance

Considering that the hybrid vehicle has one additional driven axle, allowing greater road grip utilization, one can expect that the tractor plus e-dolly combination, for any weight class, has higher traction capacity than the conventional one. This aspect must provide better performance on vehicle average speed, acceleration and thus mission time.

Gradeability

According to [24] gradeability is the maximum uphill grade that a laden vehicle is capable of sustaining at a certain speed. In addition to this description, gradeability definition will account another aspect, which is to maintain high gears. Such condition is of great interest in vehicles equipped with stepped transmissions to reduce downshift while going on uphill so the engine operates in higher efficiency zones. Gradeability was assessed only for a severe slope condition of 5 deg. All outcomes are shown below.

GCW 80 tonnes				GCW 60 tonnes			
Engine	Battery	ΔSpeed (%)	ΔGear	Engine	Battery	ΔSpeed (%)	ΔGear
D13	1BP/P/O	2.38	0	D11	1BP/P/O	17.07	1
	2BP/P/O	21.43	1		2BP/P/O	56.66	2
	1BP/E/O	-7.14	0		1BP/E/O	-12.20	1
	2BP/E/O	2.38	1		2BP/E/O	12.20	1
	3BP/E/O	21.43	1		3BP/E/O	53.66	2
	4BP/E/O	21.43	1		4BP/E/O	63.41	2

Table 6.1: Results from a 5% gradeability simulation of an A-double coupled with e-dolly and different battery types. The column $\Delta Speed$ states the difference in maximum longitudinal speed of the given hybrid combination in comparison to the reference vehicle. Column $\Delta Gear$ states the number of gears that the hybrid truck was above or below the gear of the reference vehicle. Also, $\Delta Gear$ is only assessed for the gearbox on the tractor unit. The reference parameters are from an ICE truck powered with D13 (60t) or D16 (80t) engine. Battery nomenclature: number of battery packs / power or energy / optimized.

From the table, truck gradeability is improved for almost all combinations, except if applied 1 battery pack of energy optimized to the EPS. For the 80t vehicle, a reason can be understood by observing engine specification in Tab. A.3. Comparing the maximum output power from a D16 engine with a D13 plus the battery in question, the maximum propelling power achieved by the standard vehicle is greater than the one with e-dolly (approximately 10%), resulting in a lower powertrain performance and thus a lower gradeability performance.

As the vehicle is described with a quarter car model, the whole combination weight is sustained by just one axle. Analysing equation 6.1, the maximum longitudinal force ($F_{i_x}^{max}$) that an axle can sustain before slip is directly dependent on the normal load (F_{i_z}). Therefore, in the gradeability simulation, the tyre will not slip as the available grip is too high (F_{i_z} too high). Maybe, if the grip limit was conditioned with load distribution, one could find a different result on the previous case, as the hybrid LCV has more friction available because of the extra propelled axle on the e-dolly.

$$F_{i_x}^{max} = \mu \cdot F_{i_z} \tag{6.1}$$

For the 60t combination, one cannot explain the slower speed using the same reasoning as before, thus another explanation must be addressed to this case. Observing the column *Gear*, the simulation shows that the e-dolly topology is one gear step higher than the one presented by the conventional vehicle. Since high gears give lower traction capacity, this might be causing the hybrid truck to have a lower velocity in the gradeability test. To examine this assumption, the simulation was performed again with a constraint. Now, the speed is bounded to be at least equal to the one shown by the diesel-powered truck. From the simulation the vehicle speed was 7% greater than the conventional one, but with the same gear; i.e. $\Delta Speed$ 7% and $\Delta Gear$ 0.

Average speed

Hereupon, considering that some batteries are expensive or posses either low traction or storage capacity, only two battery types were applied in the following analyses. They are, the formerly mentioned two packs of power-optimized batteries, due to the best cost-benefit ratio; and, three packs of energy-optimized batteries, as it yields the same throughput power as the two power-optimized packs but with a larger energy capacity.

In order to sustain the gradeability test and aid the average speed analysis, the longitudinal speed was plotted over the same road length for both hybrid and diesel trucks, i.e. they are subjected to the same road grade.

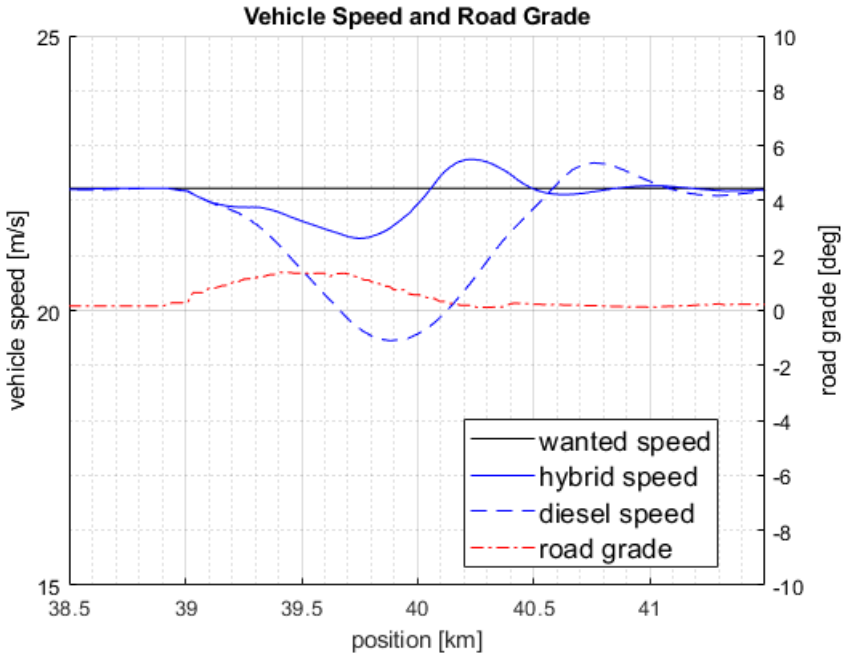


Figure 6.3: *Longitudinal speed profile of 80t trucks with (hybrid) and without (diesel) e-dolly over the same road grade and length. The hybrid vehicle posses 2 packs of power optimized batteries.*

As demonstrated by the speed profiles in Fig. 6.3, the hybrid combination sustains its velocity better than the diesel truck under the same road grade conditions. This output supports what has been presented in the previous section, that the vehicle with an additional electric drive will perform best in gradeability. Also, if the hybrid vehicle is capable of better maintaining its speed, one can assume that the same vehicle shall have a better mission average speed than the regular one. Tab. 6.2 shows a comparison between the study objects and confirms this assumption.

80 tonnes		
Battery	Charge	ΔAverage Speed (%)
2BP/P/O	No	3
	Yes	2
3BP/E/O	No	3
	Yes	3

Table 6.2: Average vehicle speed shown by 80t hybrid combinations relative to the case without e-dolly. Different hardware set-up and charging scenario are evaluated.

Gear shifting

Gear shifting involves a series of mechanical actions in the powertrain related to the motion of moving parts, e.g. clutches and gear wheels. Whenever one of these elements are engaged to or disengaged, wear occurs as a result of the relative movement of two solid surfaces. Comparing two vehicles that, for instance, have two different gear-shifting strategies, the one that performs a higher number of gear-shifts over the same cycle will show a reduced gear wheel lifetime due to wear.

Worn gears have less efficiency when compared to those unused, dissipating more power and consequently increasing fuel consumption. All these debilitating factors might lead to early product replacement yielding additional costs to the costumer. Hence, to decrease number of gear shifts performed by a transmission system is naturally stated beneficial. On this knowledge Tab. 6.3 displays the amount of gear-shifts executed by the hybrid architectures over cycle under consideration. Again, the results are compared to the reference vehicles earlier declared.

80 tonnes		
Battery	Charge	ΔGear Shifts (%)
2BP/P/O	No	-4
	Yes	-8
3BP/E/O	No	-9
	Yes	-15

Table 6.3: Percentage of gear-shifts showed by 80t hybrid combinations relative to the reference vehicle. Different hardware set-up and charging scenario are evaluated.

As expected, the hybrid truck performs less gear-shifts than the conventional one. Also, in *with charge* scenarios, lower percentages are found. The presence of a secondary propulsion system, in this case an electric motor, causes the engine to operate less than usual and so the gearbox. Furthermore, if one takes into account that a truck's lifetime is approximately 5 years, to reduce the gear-shifting by, for example, 4% on each task, this reduction might lead to a considerable impact on the costumer's total cost of ownership. Therefore, the electrified dolly favours the lifespan of moving parts and consequently total cost of ownership.

6.3 A Comparison on Vehicle Stability

In order to claim that long haul trucks coupled with e-dollies are dynamically more unstable than conventional ones, the margin grip strategy, presented in Sec. 4.2, is applied. The axles' margin grip were assessed by post-processing the data obtained from the longitudinal simulations as follows. Primarily, the functional mock-up interface is instantiated with the necessary variables from the data file, e.g. vehicle speed and the longitudinal forces on the axles. Then, the model is initialized and the grip margins are computed. The minimum margin over all axles is used to define the vehicle's minimum margin curve, displayed in Fig. 6.4. This process is done for both diesel and hybrid vehicles.

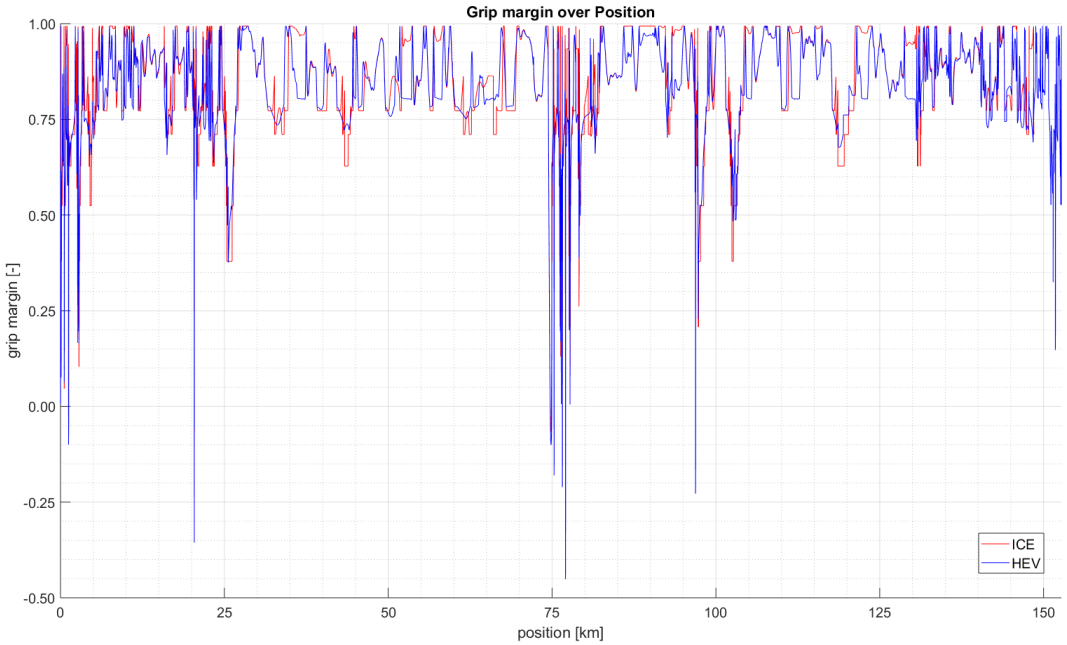


Figure 6.4: *Minimum grip margin curves of a conventional diesel truck powered with a D16 engine (ICE) and an e-dolly hybridized truck powered with a D13 engine and 2 power optimized battery packs (HEV).*

From the plot it is possible to observe that both vehicles show similarities in margin grip behaviour. Although the blue line, which represents the margin of the e-dolly combination, stands out from the red one, they shows almost the same grip depreciation when reaching low margin values. To better understand the outcomes from the post-processing a second chart was depicted in Fig. 6.5.

While cornering, lateral forces are developed on the wheels, this in turn, reduces the available grip between road and tyre, making it easier to cause wheel slip. As can be seen in the plot, whenever the driver faces a curve, which implies that a steering input is given to the wheels, the available grip decreases. One can also observe that the depreciation is proportional to the magnitude of the steering input. This observation shows that the model acts as expected, giving some reliability to the stability approach developed earlier. Summarizing from both plots, one can state that the average stability of a long combination vehicle powered with an e-dolly suffers a small depreciation in comparison to a standard vehicle not equipped with this device.

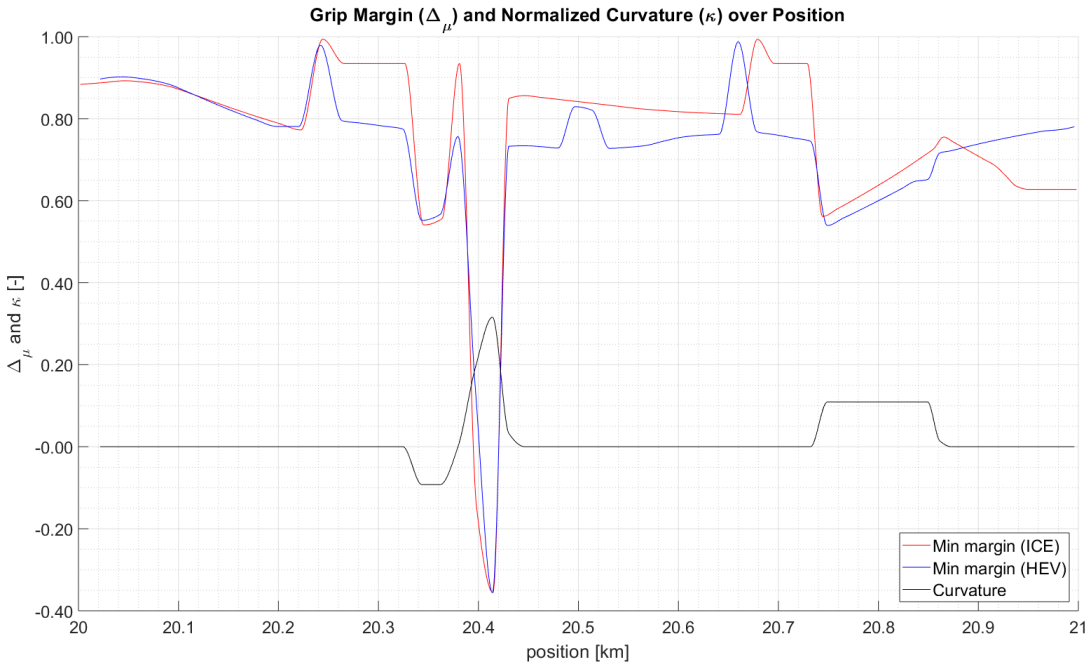


Figure 6.5: *Minimum grip margin curves and normalized curvature from a section of the operating cycle. ICE refers to the standard diesel truck and HEV to the hybrid e-dolly combination truck. The curves were smoothed using "pchip" function from Matlab.*

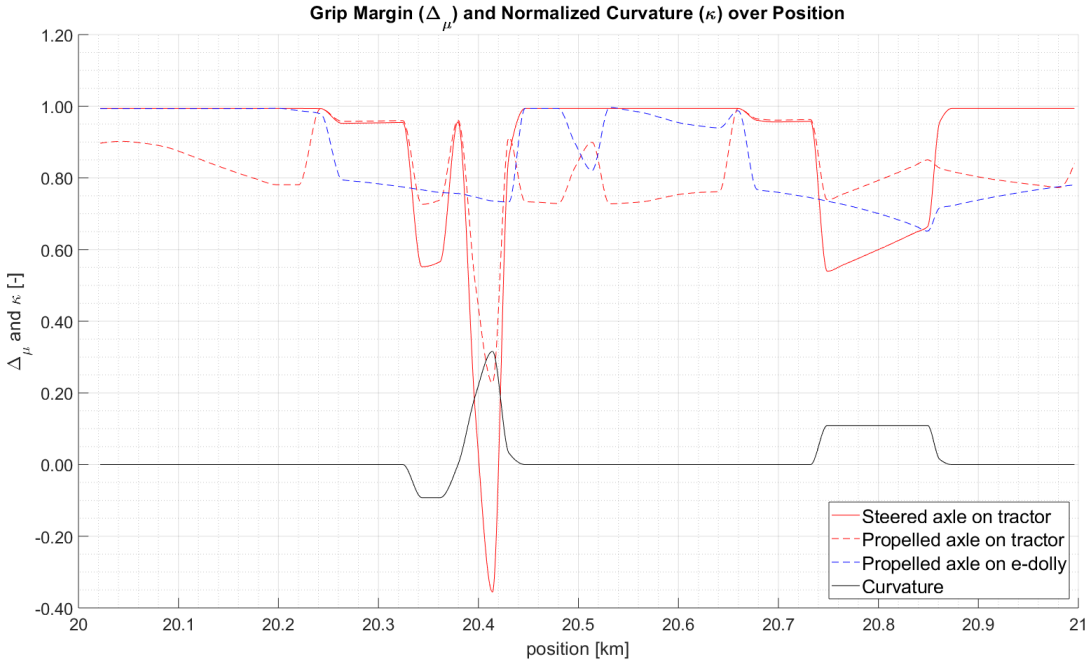


Figure 6.6: *Grip margins of the tractor's steered and propelled axles, and e-dolly's propelled axle of the hybrid combination truck. As mentioned in sec. 4.1, the e-dolly is modelled with a non-steerable axle. The curves were smoothed using "pchip" function from Matlab.*

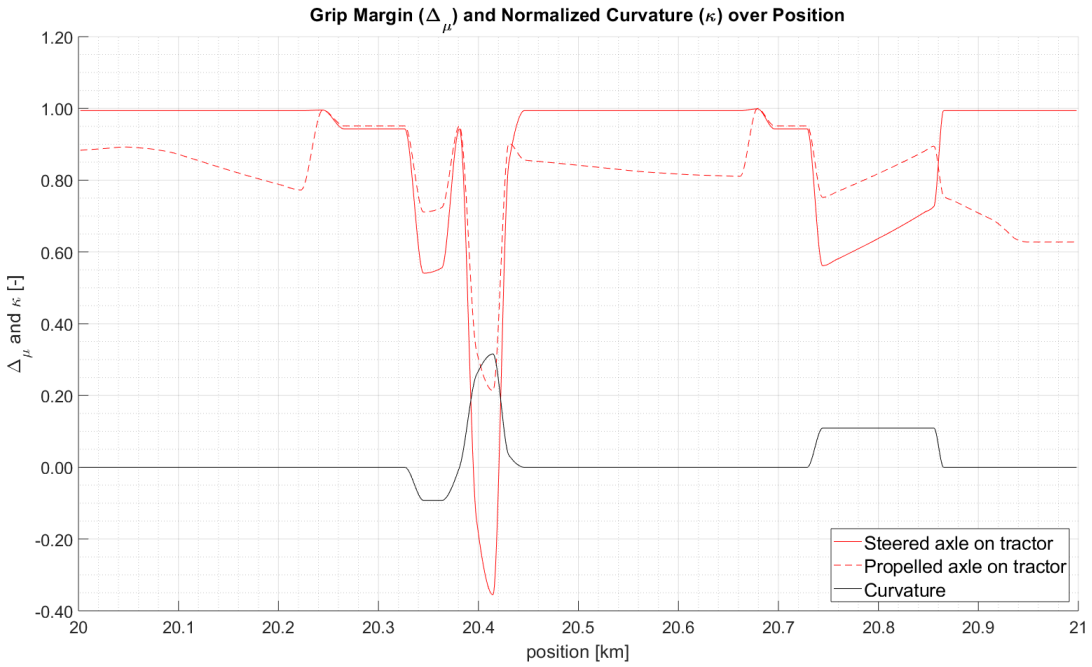


Figure 6.7: *Grip margins of the tractor's steered and propelled axles of the standard diesel truck. As mentioned in sec. 4.1. The curves were smoothed using "pchip" function from Matlab.*

Considering the margin behaviour of the selected axles displayed in Fig. 6.6 and Fig. 6.7, one can state that the steered axle is the one most responsible for depreciating the truck's minimum grip margin curve, illustrated in Fig. 6.5. Also, is possible to imply that the lateral stability of the vehicle plus e-dolly combination is not heavily affected by the extra propelled axle. The main difference between a truck with and without an e-dolly is the axle responsible for lowering the margin grip, which changes between the ICE and EM propelled axles according to the power split actions, depicted in the last two plots.

6.4 The Influence of the Stability Constraint on Control Decisions

To identify how the stability constraint affects the control unit power split decision, simulations were performed with and without the margin grip limitation within the control algorithm. The objective is to detect any changes in the split action performed by the controller and verify if these changes have substantial discrepancy to the usual actions. Such knowledge will point out where longitudinal models, generally used to estimate fuel consumption, are strongly affected, or not, by the dynamics of the truck. To perform this analysis, a segment of the cycle, which includes steering inputs and both powertrains usage, was chosen. The diagram below shows how the power distribution behaves for each control strategy. Also, both algorithms must supply the same amount of energy, demanded by the driver, so a fair comparison is made.

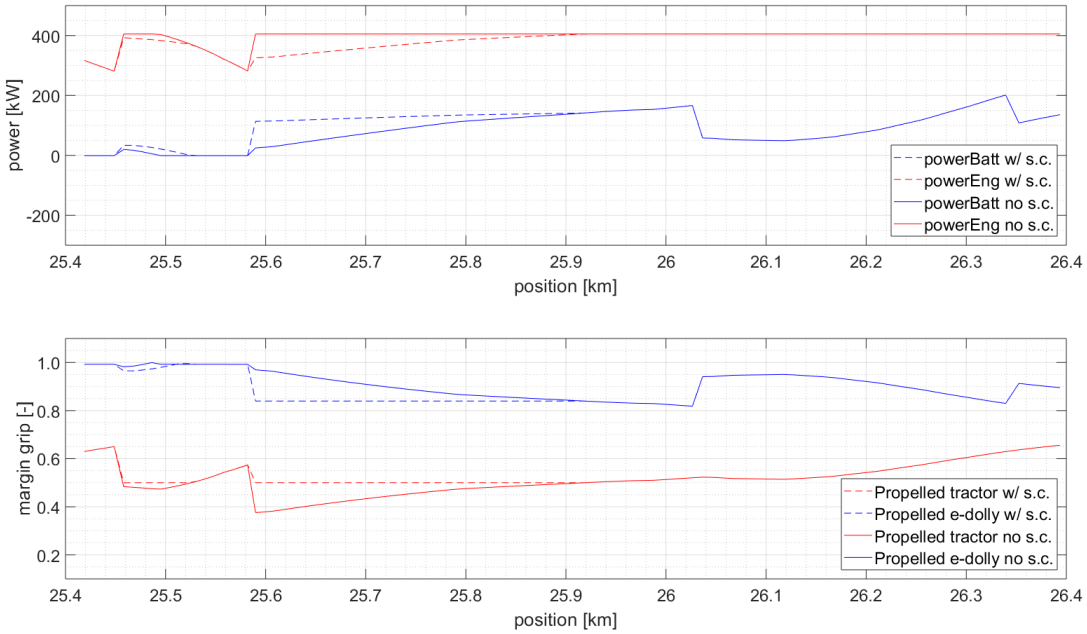


Figure 6.8: *Simulation results of a vehicle using two different control strategies (with and without stability constraints). Upper diagram: battery and engine output power over position. Lower diagram: tractor and e-dolly propelled axles' grip margins over position. "s.c." stands for stability constraint and "w/" for with.*

In the diagram, the blue color is used to represent variables associated to the e-dolly, i.e. the battery output power and the margin grip of the electrically propelled axle. The red colour, in the other hand, represents variables related to the tractor unit. Moreover, dashed lines characterize split decisions made considering the stability constraint (Eq. 3.13), while the continuous ones refer to split decisions without this constraint.

Considering the case scenario where no stability constraint is used, the tractor's propelled axle Δ_μ is below the threshold, approximately 0.38 at 25.6 *km*. However, examining the margin curve of the e-dolly's propelled axle, considerable grip is available for usage by that axle, which could be used to assist the first axle. After implementing the grip constraint in the algorithm, a different split action is picked by the control unit. Now, the engine supplies less energy than before, increasing the grip margin of the tractor's propelled axle. The opposite happens to the battery, which is used to supply the remaining energy demand from the driver.

Paying attention to the figure, one may notice that both diagrams show a mirrored behaviour. This can be motivated as follows. The grip margin is inversely proportional to both longitudinal and lateral forces. These are mainly developed from the input power and the steering angle given to the wheel, respectively. Therefore, if the lateral forces are kept constant (i.e. no steering input) and the power decreases, the longitudinal force over the axle will also decrease. Thus, the grip margin will increase. Also, the margin will display a mirrored behaviour to any oscillation in power. See Fig. 6.8.

To better understand how the controller make its decisions, a single time step that bears an unstable event was used to demonstrate how the power distribution changes due to the inclusion of the grip margin constraint.

Table 6.4 displays the actions taken by the control system and the respective outcomes.

Split Decisions			
Variable	With Lat. Control	Without Lat. Control	Unit
P_{dem}	370	370	kW
$P_{delivered}$	418	410	kW
P_{batt}	87	5	kW
P_{eng}	331	405	kW
Δ_{μ}	+10.35	-9.81	%

Table 6.4: The difference in the power split decisions made by two control units, in which one of them does not consider the vehicle's lateral stability and where the same input conditions are given.

Observing the results, when the controller neglects the grip constraint, almost all power demand is supplied by the engine. This, in turn, causes the available grip in the tractor's wheel to go below the threshold, indicating that the wheel is either slipping front or side ways, converting power into heat and wearing the tyre. In contrast, the case *with lateral constraint* shows that the control unit adopted a different split decision in order to maintain the tyre grip above the threshold. This was done by using the electric axle to aid the diesel-powered one, keeping the grip of the tractor propelled axle in a safe region.

Summarizing, once the grip margin is used as a constraint in the optimization problem, different split decisions are made. Therefore, one can claim that, stability constraints do affect the control unit's power split decisions. However, these decisions only differ in particular sections of the operating cycle, e.g. during unstable events. Knowing that these events are sporadic, one can also claim that, for simulations whose objective is to estimate energy consumption, these different split decisions might not produce a significant impact on the final result.

6.5 The Influence of Drawbar Limitations on the Control Decision

Regarding deliverable 4, in section 1.4, an expression is proposed to estimate stresses on drawbar couplings. To implement the equation as a constraint in the optimization algorithm, without increasing its run-time, the expression is made explicit and simple. Represented by Eq. 6.2, this expression only computes the longitudinal force on the coupling joint as drawbars are often subjected to longitudinal pushing and pulling forces. The equation requires the vehicle mass distribution, where m_e is the mass pulled by the e-dolly and m_t the mass pulled by the tractor unit, and the forces acting on the axles (F_{i_x}) as inputs. Appendix B demonstrates how it was obtained using a free-body diagram of the articulated truck.

$$F_d = \frac{(F_{1_x} + F_{2_x} + F_{3_x} + F_{4_x} + F_{5_x} + F_{6_x}) \cdot (\frac{m_e}{m_t}) - (F_{7_x} + F_{8_x} + F_{9_x} + F_{10_x} + F_{11_x})}{1 + (\frac{m_e}{m_t})} \tag{6.2}$$

The equation above intends to help the designer in two ways. First, to judge whether or not a drawbar model supports the loads arising from the motion of the truck (in the given cycle). This is done by knowing the magnitude of the forces acting on the drawbar (F_d). Second, to understand how the control unit (optimization algorithm) will perform with additional constraints.

The plots on Fig. 6.9 and 6.10 are from two different simulations, they differ in the force allowed on the coupling point. The plots in the first figure were acquired applying a limit of 100 *kN* to the drawbar stress, and the ones in the second figure, 20 *kN*. By presenting the power distribution and the drawbar force it is possible to understand the influence of the studied constraint on the control unit decision making and to verify the proposed model.

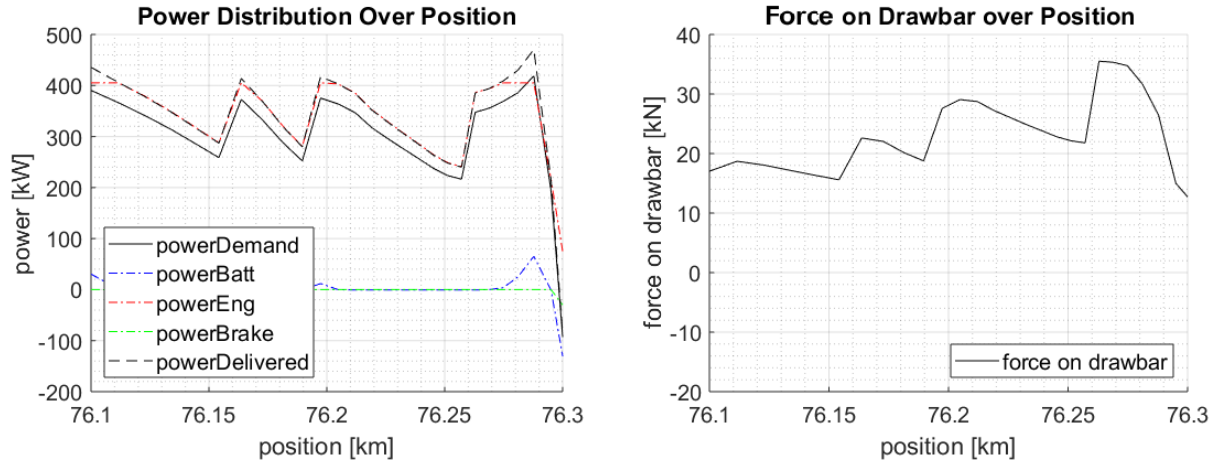


Figure 6.9: *Simulation results of power distribution and force on the drawbar over position for a component with mechanical limit of 100 kN.*

Observing the left chart on Fig. 6.9, the propelling power is mostly given by the ICE (dotted red line). According to the plot on the right side, this split decision leads to coupling forces greater than 30 *kN*, which is below the 100 *kN* bound settled in the simulation. If the limit is changed to 20 *kN*, the controller shall decide for a different split distribution to keep the drawbar stress below the new threshold. On Fig. 6.10, the second scenario (20 *kN*) is addressed. From the left-hand side picture, one can realize that the controller avoided reaching the new threshold by changing the output power of both ICE and EM, i.e. propelling the vehicle's second-half with the e-dolly, thus the tractive force acting on the drawbar joint is diminished and the constraint satisfied as shown in the right-hand side of Fig. 6.10. This short comparison depicts the effectiveness of the proposed formulation. Also, this shows how a control system can be shaped to reach some objectives through implementation of new constraints.

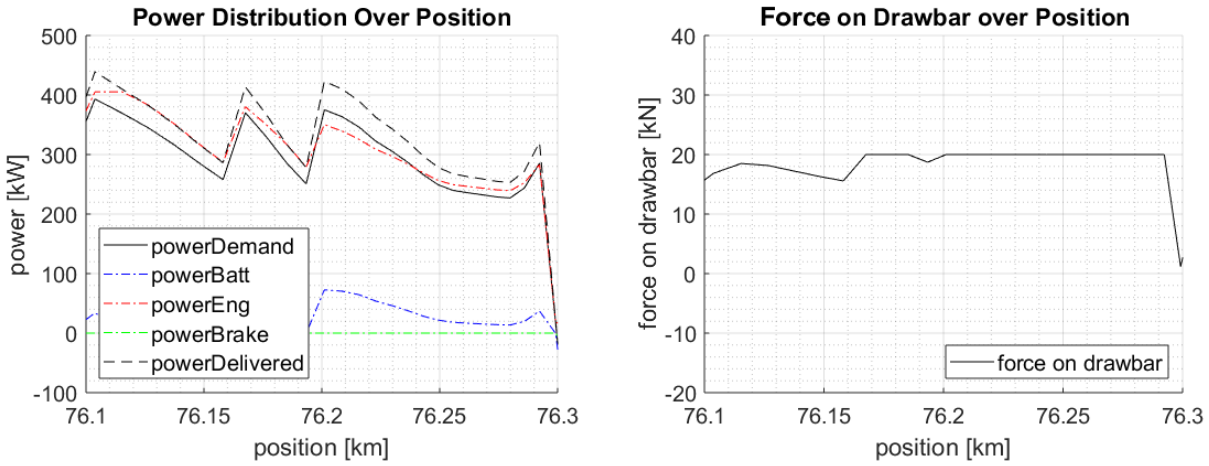


Figure 6.10: *Simulation results of power distribution and force on drawbar over position for a component with mechanical limit of 20 kN.*

Fig. 6.11 delineates how the drawbar experiences stresses throughout the cycle. Inspecting the peaks one will notice that the mechanism by no means reaches the threshold of the drawbar inspected in this thesis with mechanical limit of, approximately, 100 *kN*. Furthermore, the peak value has a magnitude three times lower than the upper bound, thus one can imply that the safety factor of the component, assessed for the hardware set-up described in the figure, is close to 3. Such a value of safety factor is commonly used for mechanical components of heavy duty trucks. Therefore, one might assume that the equation is reasonable.

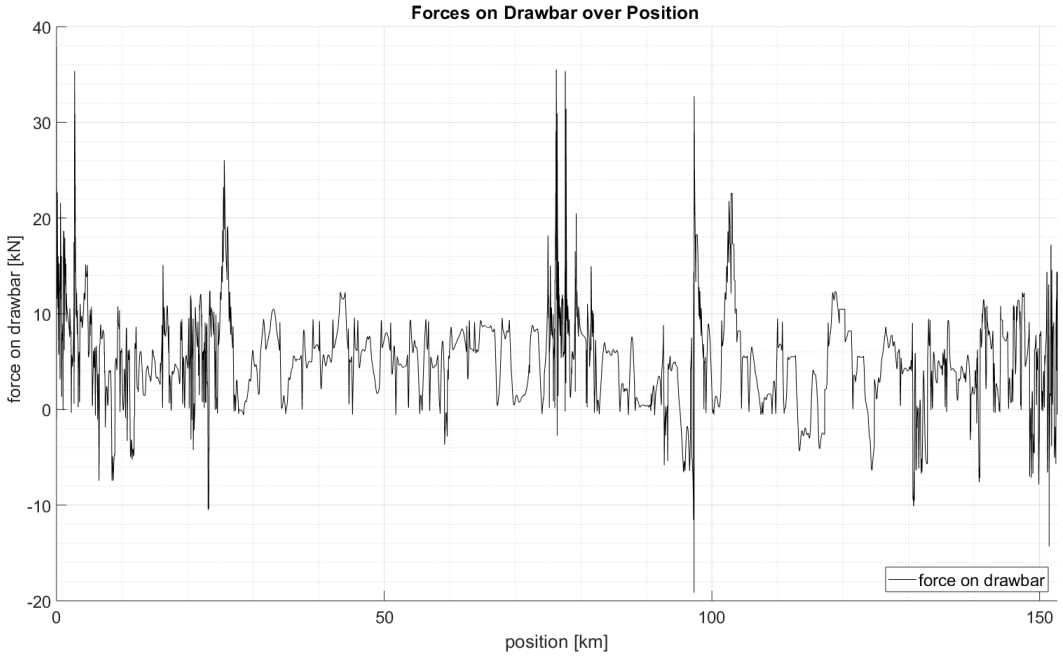


Figure 6.11: *Force on drawbar due to propulsion and brake of the combination vehicle over position. The drawbar constraint is set to 100 kN.*

In addition to the previous analyses, the fuel consumption was also compared. Again, both study cases were assessed (20 *kN* and 100 *kN*). It can be seen from Fig. 6.11 that, for most of the cycle, the force on the drawbar remains below 20 *kN*. Therefore, if the force allowed on the drawbar is reduced to 20 *kN*, one expects that the power split decisions will not change much as well as the fuel consumption in comparison to the 100 *kN* case. The simulation results show that, if the bound is set to 20 *kN*, the vehicle consumes 1% more fuel

than the other study case, which is reasonable considering the presumption afore mentioned.

7 Conclusion

This thesis provided an overview of the e-dolly concept and explored how it affects the energy consumption and powertrain performance of long haul trucks. Furthermore, it was investigated how vehicle stability constraints change power split decisions made by the control unit of a hybrid vehicle. A forward simulation model and an adaptive ECMS controller was used and described in this thesis work. In the study case a short set of batteries were assessed.

According to the results, the e-dolly technology is a promising feature for heavy duty trucks. Vehicles powered with this system and equipped with a downsized engine show good fuel savings, approximately 16% considering an e-dolly with two power optimized battery packs, and better performance in almost all aspects of vehicle capabilities, i.e. $\sim$21% in gradeability, $\sim$3% in average speed and $\sim$-4% of gear-shifts.

As regards vehicle stability, the analysis performed in Sec. 6.4 showed that stability constraints do affect control decisions, however, only during unstable events, which are a few in the evaluated cycle. The high computation time, the complex formulation and the low impact of a control algorithm that considers stability constraints does not encourages the application of this approach in simulations that, for instance, are used to estimate energy consumption of vehicles performing a distribution task. However, the presented approach may be useful to understand how the control unit must act in manoeuvres that might cause instability.

8 Future Work

The analysis carried out in this work verifies the performance of LCVs combined with electrified dollies, but performance does not always mean profitability as mentioned in section 6.1. For this reason, a total cost of ownership investigation shall be conducted on the given combinations, so that, from a financial perspective, one can identify in which occasions a conventional truck would benefit from the e-dolly application. Along with this study, future scenarios could also be evaluated, considering that fuel price and taxes might increase for ICE driven vehicles while fees, battery and electricity costs might decrease for electric and hybrid vehicles in the forthcoming years due to fiscal incentives and progress in battery technology.

In order to improve the control decisions and the accuracy of the simulation results, specially concerning the vehicle fuel consumption, an optimal target curve for the state of charge must be obtained. This can be accomplished using optimization algorithms. Then, the new SOC target can be fixed in the software so global optimum actions are made by the controller. Furthermore, due to the adaptive control, it would be possible to verify (with other simulation frameworks, e.g. Volvo's simulation platform) how the control and active safety systems behave when the vehicle is subjected to lane change or rollover scenarios.

The system of equations that represents the vehicle's lateral dynamics shall also be enhanced to a two-track model as rollover scenarios are better described with this kind of assumption. Moreover, the tyre model must be changed to a more refined model, such as the magic tyre formula [25], to better describe the contact between tyre and road surfaces, and thus stability. Concerning the powertrain models, to select advanced gear-shift and brake strategies might improve the overall simulation reliability. The last, but not least, would be to develop an explicit expression to assess the tyre grip margin that could be implemented directly in Matlab scripts, without the necessity of using FMUs, thereby decreasing computational time and reducing the amount of software/licenses required to perform this type of simulation.

References

[1] *Greenhouse gas emissions from transport*. European Environmental Agency. URL: https://www.eea.europa.eu/data-and-maps/indicators/transport-emissions-of-greenhouse-gases/transport-emissions-of-greenhouse-gases-10.

[2] *Dolly*. NTI. URL: https://www.nti.com.au/images/truck-and-trailer/types/img_72_lg.jpg.

[3] B. de Jager, T. van Keulen, and J. Kessels. *Optimal Control of Hybrid Vehicles*. Springer, 2013.

[4] T. Ghandriz. "Optimization Based Design of Heterogeneous Truck Fleet and Electric Propulsion". IEEE: International Conference on Intelligent Transportation Engineering. Gothenburg, Sweden: Chalmers University of Technology, 2016.

[5] B. Jacobson et al. *Vehicle Dynamics*. Chalmers University of Technology, 2017.

[6] J. Aurell and T. Wadman. "Vehicle combinations based on the modular concept". Report. Sweden: Volvo Trucks, 2007.

[7] P. Pettersson. "On Numerical Descriptions of Road Transport Missions". Thesis for the Degree of Licentiate of Engineering in Machine and Vehicle Systems. Gothenburg, Sweden: Chalmers University of Technology, 2017.

[8] P. Pettersson, B. Jacobson, and S. Berglund. "Model for automatically shifted truck during operating cycle for prediction of longitudinal performance". Report. Gothenburg, Sweden: Chalmers University of Technology, 2016.

[9] S. Knupfer et al. *How automakers can drive electrified vehicle sales and profitability*. McKinsey and Company, 2017.

[10] A. Berrueta et al. "Comparison of State-of-Charge Estimation Methods for Stationary Lithium-Ion Batteries". IEEE. Pamplona. Spain: Public University of Navarre, 2016.

[11] J. Schmalstieg et al. "A holistic aging model for Li(NiMnCo)O2 based 18650 lithium-ion batteries". Journal of Power Sources. Germany: RWTH Aachen University, 2014.

[12] J. Schmalstieg et al. "A holistic aging model for Li(NiMnCo)O2 based 18650 lithium-ion batteries". Journal of Power Sources, 2014.

[13] I. Mareev, J. Becker, and D. U. Sauer. "Battery Dimensioning and Life Cycle Costs Analysis for a Heavy-Duty Truck Considering the Requirements of Long-Haul Transportation". Energies, 2018.

[14] S. Onori, L. Serrao, and G. Rizzoni. *Hybrid Electric Vehicles. Energy Management Strategies*. Springer, 2016.

[15] P. Papalambros and D. Wilde. *Principles of optimal design: modeling and computation*. Cambridge University, 2000.

[16] *IHP radial flux motor*. URL: https://www.researchgate.net/figure/fig1_283776745.

[17] L. Serrao, S. Onori, and G. Rizzoni. "ECMS as a realization of Pontryagin's minimum principle for HEV control". American Control Conference. Saint Louis, U.S.A., 2009.

[18] R. Englund. "Setting the Equivalence Factor in Equivalent Consumption Minimization Strategy using Reinforcement Learning Based Controller". MA thesis. Gothenburg, Sweden: Chalmers University of Technology, 2017.

[19] M. Sivertsson, C. Sundström, and L. Eriksson. "Adaptive Control of a Hybrid Powertrain with Map-based ECMS". IFAC World Congress 2011. Linköping: Linköping University, 2011.

[20] T. Ghandriz. "Sensitivity Analysis of Optimal Energy Management in Plug-in Hybrid Heavy Vehicles". IEEE: International Conference on Intelligent Transportation Engineering. Gothenburg, Sweden: Chalmers University of Technology, 2017.

[21] C. Winkler, P. Fancher, and C. MacAdam. "Parametric Analysis of Heavy Duty Truck Dynamic Stability". Technical Report. Ann Arbor, Michigan: The University of Michigan, 1983.

[22] P. Sundström. "Vectorized single-track model in Modelica for articulated vehicles with arbitrary number of units and axles". MA thesis. Chalmers University of Technology, 2014.

[23] B. Jacobson et al. "An Open Assessment Tool for Performance Based Standards of Long Combination Vehicles". Research report. Gothenburg, Sweden: Chalmers University of Technology, 2017.

[24] M. S. Kati. "Definitions of Performance Based Characteristics for Long Heavy Vehicle Combinations". Report. Gothenburg, Sweden: Chalmers University of Technology, 2013.

[25] H. Pacejka. *Tire and Vehicle Dynamics*. 3rd ed. Elsevier, 2012.

[26] *Volto Trucks, Driveline Specifications*. URL: https://www.volvotrucks.co.uk/en-gb/trucks/volvo-fh/specifications/driveline.html.

Appendices

A Data

Battery Specification							
Label	1BP-PO	2BP-PO	1BP-EO	2BP-EO	3BP-EO	4BP-EO	Unit
E_{batt}	33	66	170	340	510	680	MJ
P_{min}	-150	-300	-100	-200	-300	-400	kW
P_{max}	150	300	100	200	300	400	kW
V_{nom}	3	3	3.5	3.5	3.5	3.5	V
$n_{cell/pack}$	200	200	360	360	360	360	-
R_{cell}	0.003	0.003	0.004	0.004	0.004	0.004	Ω

Table A.1: Batteries characteristics. BP - Battery Packs; P - Power; E - Energy; O - Optimized.

Mass Distribution					
80t	9841	33101	3200	33800	kg

Table A.2: Distribution of the Vehicle mass on each unit. They are, the tractor, first semi-trailer, dolly and second semi-trailer respectively.

Engine Specification			
Engine	Max Power (kW)	Max Torque (Nm)	Max Exhaust Braking Power (kW)
D11K450	332	2150	160
D13K540	397	2600	200
D16K750	552	3550	230

Table A.3: Engine specifications. Table's contents are public records, i.e. not confidential, available in [26].

B Drawbar Constraint

This appendix shows how to obtain a simplified expression to estimate the forces on a drawbar (F_d). The coupling mechanism is represented as a point where pulling and pushing forces can act on (Fig. B.1). These forces are derived from the action and reaction forces of i) the first-half of the A-double, i.e. tractor and trailer ($F_{d_{tractor}}$), and ii) the second-half of the A-double, i.e. converter dolly and semi-trailer ($F_{d_{dolly}}$). The coordinate system used to derive the expression is in accordance to ISO 8855.

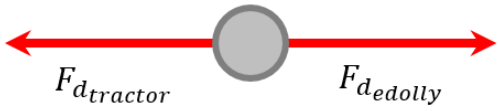


Figure B.1: *Free-body diagram of the drawbar and acting forces.*

Based on the Free-Body Diagram (FBD) above, an equilibrium equation is derived as follows,

$$F_{d_{tractor}} - F_{d_{dolly}} = 0$$
$$F_{d_{tractor}} = F_{d_{dolly}} = F_d$$

In order to find the contribution of $F_{d_{tractor}}$ and $F_{d_{dolly}}$ the problem is split between each half of the combination vehicle. First, the load contribution from the tractor side will be addressed. The FBD is shown in Fig. B.2.

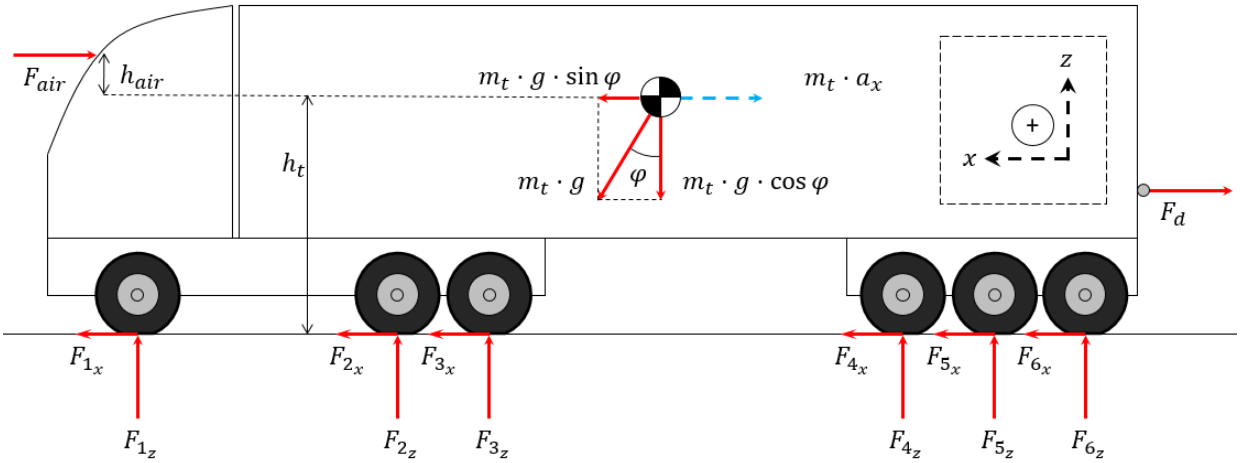


Figure B.2: *Free-body diagram of the first-half of an A-double truck. The tractor unit and trailer are visualized. m_t is the tractor's pulling mass*

Applying equilibrium on the longitudinal (x) direction the following equation is found. Here, "φ" is the road grade, "g" is the acceleration of gravity, "m_t" is the mass pulled by the tractor unit, "F_{air}" is the air drag resistance, "F_{i_x}" is the force on the axle and "a_x" the vehicle's longitudinal acceleration.

$$F_{1_x} + F_{2_x} + F_{3_x} + F_{4_x} + F_{5_x} + F_{6_x} + (\sin\varphi \cdot m_t \cdot g) - (m_t \cdot a_x) - F_{air} - F_d = 0$$

To derive the forthcoming explicit equation for F_d a common variable shared by both sides of the vehicle is needed. Here a_x is adopted. Thus, rearranging the previous expression for a_x,

$$a_x = \frac{F_{1_x} + F_{2_x} + F_{3_x} + F_{4_x} + F_{5_x} + F_{6_x} + (\sin\varphi \cdot m_t \cdot g) - F_{air} - F_d}{m_t}$$

Before proceeding, a second equation is needed. Doing the analysis of the dolly contribution (see Fig. B.3) a second equilibrium equation is obtained.

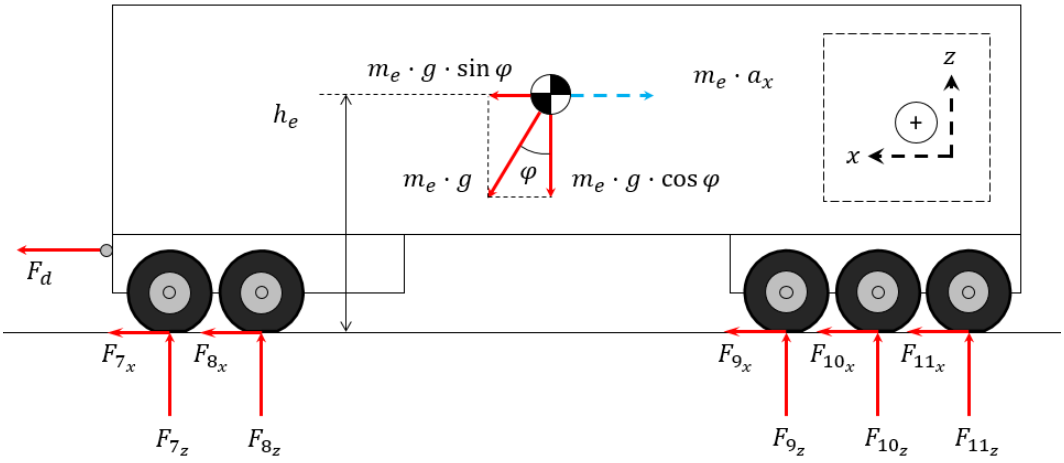


Figure B.3: *Free-body diagram of the second-half of an A-double truck. The dolly unit and semi-trailer are visualized. m_t is the e-dolly's pulling mass*

From the equilibrium the equation below is found. "m_e" is the mass pulled by the e-dolly.

$$F_{7_x} + F_{8_x} + F_{9_x} + F_{10_x} + F_{11_x} + (\sin\varphi \cdot m_e \cdot g) - (m_e \cdot a_x) + F_d = 0$$

Again, rearranging the equation for a_x.

$$a_x = \frac{F_{7_x} + F_{8_x} + F_{9_x} + F_{10_x} + F_{11_x} + (\sin\varphi \cdot m_e \cdot g) + F_d}{m_e}$$

Now, there are two equations for a_x function of F_d. Matching both, a general expression can be reached.

$$\frac{F_{1_x} + F_{2_x} + F_{3_x} + F_{4_x} + F_{5_x} + F_{6_x} + (\sin\varphi \cdot m_t \cdot g) - F_{air} - F_d}{m_t} = \frac{F_{7_x} + F_{8_x} + F_{9_x} + F_{10_x} + F_{11_x} + (\sin\varphi \cdot m_e \cdot g) + F_d}{m_e}$$

and therefore,

$$(F_{1_x} + F_{2_x} + F_{3_x} + F_{4_x} + F_{5_x} + F_{6_x} + (\sin\varphi \cdot m_t \cdot g) - F_{air} - F_d) \cdot (\frac{m_e}{m_t}) = F_{7_x} + F_{8_x} + F_{9_x} + F_{10_x} + F_{11_x} + (\sin\varphi \cdot m_e \cdot g) + F_d$$

The influence of the road slope can be canceled out and the air drag neglected.

$$(F_{1_x} + F_{2_x} + F_{3_x} + F_{4_x} + F_{5_x} + F_{6_x} - F_d) \cdot (\frac{m_e}{m_t}) = F_{7_x} + F_{8_x} + F_{9_x} + F_{10_x} + F_{11_x} + F_d$$

Isolating F_d the final expression is acquired.

$$F_d = \frac{(F_{1_x} + F_{2_x} + F_{3_x} + F_{4_x} + F_{5_x} + F_{6_x}) \cdot (\frac{m_e}{m_t}) - (F_{7_x} + F_{8_x} + F_{9_x} + F_{10_x} + F_{11_x})}{1 + (\frac{m_e}{m_t})} \tag{B.1}$$

Eq. B.1 is used as a constraint in the optimization algorithm.